sustainability

MDPI

Article

Delineation of Salinization and Recharge Sources Affecting Groundwater Quality Using Chemical and Isotopic Indices in the Northwest Coast, Egypt

Hesham A. Ezzeldin

Hydrogeochemistry Department, Desert Research Center, Cairo P.O. Box 11753, Egypt; h.ezzeldin@drc.gov.eg or h.ezzeldin@hotmail.com

Abstract: Salinization of coastal aquifers is a serious issue affected by climate change and enhanced by overexploitation of groundwater resources. This research aims to explore the hydrogeochemical processes that cause salinization of groundwater in coastal aquifers, such as the area located between Barrani and Baqbaq, on the northwestern coast of Egypt. Various techniques were applied, including Gibbs plots and hydrochemical facies diagrams (HFE-D), ion ratios and stable isotope bivariate plots, statistical analyses, a groundwater quality index for seawater intrusion (GQI_{SWI}), and a seawater mixing index (SMI). Based on the total dissolved solids (TDS), groundwater can be classified into four groups: slightly saline (9%), moderately saline (45%), highly saline (43%), and salty water (3%). The geochemical properties were further catergorized on the basis of other parameters and ion ratios, such as Ca_{excess}, $Na_{deficit}$, Na/Cl, Cl/HCO_3, and Br/Cl, which suggest the influence of cation exchange, seawater, and marine sediment dissolution. Additionally, stable isotopes indicated two groups. One of these has relatively high salinity and low isotopic content and is affected by the leaching and dissolution of marine deposits. The other group is enriched in $\delta^{18}O$ and δD content, with much higher salinity due to mixing with seawater and evaporation. The GQI_{SWI} categorizes groundwater as saline and mixed (55 and 41%, respectively), followed by saltwater (4%), whereas the SMI calculations indicate that about 10% of the groundwater samples are impacted by seawater. Finally, the areal distribution of GQI_{SWI} and SMI identified some patches along the coastline as well as other inland places located about 12.5 km away from the sea that have undergone saltwater intrusion. In conclusion, overexploitation of groundwater should be avoided because the amount of annual rainfall is very limited.

Keywords: groundwater salinization; ion ratios; stable isotopes; seawater mixing index (SMI); northwest coast

Citation: Ezzeldin, H.A. Delineation of Salinization and Recharge Sources Affecting Groundwater Quality Using Chemical and Isotopic Indices in the Northwest Coast, Egypt. *Sustainability* **2022**, *14*, 16923. https://doi.org/10.3390/su142416923

Academic Editors: Mohamed El-Alfy, Ahmed El Kenawy, Petra-Manuela Schuwerack and Zhongfeng Xu

Received: 27 September 2022
Accepted: 8 December 2022
Published: 16 December 2022

1. Introduction

Water demand has increased, especially in coastal areas, with the rapid growth of residential, agricultural, industrial, and tourism activities. Coastal aquifers are considered one of the main sources of freshwater supplies in many countries worldwide, especially in the Mediterranean [1]. The geological heterogeneity as well as spatial and temporal variability in flow patterns play a critical role in governing the distribution of fresh and saline waters in the coastal aquifers [2]. Salinization of groundwater takes place in many coastal aquifers [3–5]. It has been found through previous studies that sources and causes of groundwater salinization in coastal aquifers are due to several processes. Among these are water–rock interactions, cation exchange, redox reactions, carbonate and evaporate mineral dissolution, wastewater disposal, and intrusion of fossil seawater and modern seawater induced by groundwater overexploitation [6–9]. All of these are linked to climate change's effects on precipitation and patterns of recharge as well as to evapotranspiration, which in turn puts pressure on the coastal aquifer systems. This likely speeds up the quantitative and qualitative degradation of groundwater. Therefore, in order to support

the sustainable management of coastal resources in the near future, it is urgent that we enhance our understanding of the spatial distribution of groundwater salinity and the factors controlling changes [10].

The most important process that degrades groundwater quality in coastal areas is the excessive abstraction of groundwater, which reduces freshwater discharge to the sea and creates a local water table depression, causing seawater upwelling [11–13]. This phenomenon is known as seawater intrusion, and it is considered one of the main reasons limiting the use of groundwater in coastal areas. When reviewing the literature around the world, it was found that the phenomenon of seawater intrusion has been documented in North America [14,15], Australia [16], Europe [17], South America [18], and Africa [19]. Recently, developing countries along the Mediterranean Sea in North Africa are facing environmental pressures resulting from high population growth, rapid urbanization, and insufficient water sector services, which necessitate identifying effective solutions to address these problems [20,21].

Many authors have conducted regional geomorphological studies on the Northwestern coast of Egypt, [22–24]. The geology and subsurface geology were also studied by others [25–27]. AbdelMogheeth [28] and Atwa [29] studied the hydrogeology and water resources of the Northwestern coastal zone, focusing on hydrogeology and hydrochemistry. Additionally, the hydrogeology of the El-Salloum area, located to the west of the study area, was investigated by Salem and Mohamed [30], who concluded that the main water bearing formation is of Middle Miocene age. Other studies in the Mediterranean basin concluded that water resources are primarily found in alluvial Pleistocene aquifers connected with stream deltas and within karst aquifers scattered across elevated coastline ridge zones [31]. Groundwater extraction from the Pleistocene oolitic and Miocene fractured limestone aquifers is the primary source of freshwater supply in the study area. Such aquifers receive significant recharge during the winter, where depressions extending between elongated coastal ridges serve as sites for groundwater replenishment [32]. Two types of factors primarily affect the chemical evolution of groundwater during flow: natural and anthropogenic activities. Natural factors include aquifer lithology, geological structures, and recharge conditions. Anthropogenic activities primarily relate to agricultural intensity, industrial and/or sewage water discharge, and groundwater overexploitation, which in turn take part in groundwater salinization, especially in coastal aquifers [33,34].

The sources and mechanisms of the groundwater salinization must be evaluated for the effective management of groundwater resources, especially in arid and semi-arid regions. However, various sources of salinity make determining the origin and mechanism of groundwater salinization extremely complex [35]. There are many factors that cause seawater intrusion, namely aquifer properties, anthropogenic activities, recharge rates, variable density flow, and effects relating to global climate change, such as higher surface air temperature, lower annual precipitation, and sea level rise. The multiplicity of such effects makes seawater intrusion a complicated hydrogeological process [36–39]. Therefore, the use of groundwater chemistry and stable isotopes (such as $\delta^{18}O$ and $\delta^{2}H$) along with the previous geophysical and hydrogeological studies is very useful to identify groundwater recharge sources as well as to assess the geochemical processes that lead to groundwater quality deterioration in arid regions [40–42]. Additionally, stable oxygen-18 and deuterium isotopes can be considered among the tools used in water management, as they are used to identify factors affecting groundwater quality such as evaporation, precipitation, and mixing processes [43,44]. A basic assumption in the use of isotopic and chemical techniques in tracking sources of salinization is that the fingerprint of the original source is preserved during the salinization process [45]. However, the original isotopic composition, as well as the chemical composition of the salinity source, could change as a result of evaporation, dilution, mixing, or rock–water interactions. For this reason, chemical and isotopic signatures of reference waters as end members (such as seawater, rainwater or paleo-groundwater) should be monitored in the studied groundwater. To achieve the main objective of this study, multiple approaches, such as hydrochemical facies

evaluation, ion ratio relationships, statistical techniques, and salinity mixing indexes are applied for a realistic interpretation of the results. This work aims to shed light on the causes of groundwater salinization and propose some solutions to mitigate or limit the aggravation of such problems. The overarching goal of this work is to help better predict, manage, and respond to environmental contaminants that threaten human health. In light of this, a clearer picture will be provided to decision-makers and/or water authorities that enables them to take the necessary measures and precautions to confront such problems.

2. Study Area

The study area extends from Sidi Barani in the east to Baqbaq in the west, for a distance of about 35 km. It extends also for about 9 km south of the Mediterranean shore line, as shown in (Figure 1). It lies between Latitudes 31°15′00″ and 31°40′00″ N and Longitudes 25°25′00″ and 26°25′00″ E, with an area of about 32 km^2.

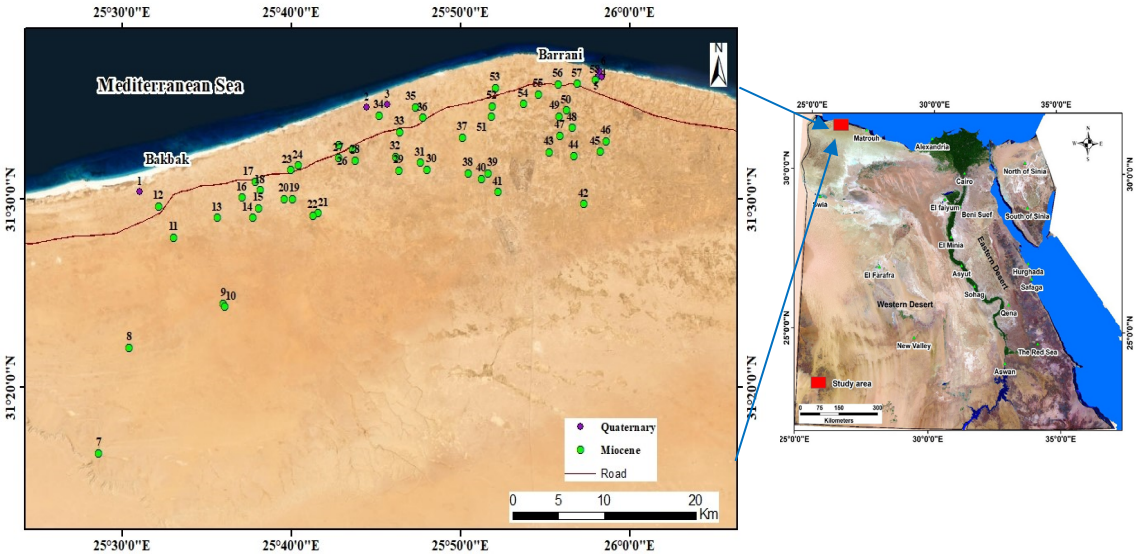

Figure 1. Study area showing the geographic location of the sampled groundwater wells (the sampling points are shaded purple for the Quaternary aquifer, while those related to the Miocene aquifer are shaded green).

3. Geomorphological and Geological Aspects

Geomorphologically, the landforms within the study area reflect the influences of endo-genetic factors (e.g., faulting, folding, lithologic features, etc.) and exo-genetic factors (e.g., climatic conditions, weathering, deposition, erosion, etc.) [46,47]. These factors result in the emergence of various landforms, such as tablelands, ridges, depressions, and dunes as well as drainage lines, all of which are affected by the distribution of surface runoff in addition to the accumulation and storage of groundwater. Three main geomorphologic units were identified: the southern tableland, the piedmont plain, and the coastal plain [27] (Figure 2). The southern tableland extends southwards to the Qattara Depression, with a maximum elevation of 250 m above sea level. The northern bounding slopes of this tableland are usually dissected by the drainage lines that discharge to the coastal plain. The piedmont plain, with low land and hills, is a transitional zone between the tableland to the south and the coastal plain to the north. Its elevation ranges from 30 to 90 m above sea level, while it varies between 2 and 25 kilometers wide. The inland depressions can be seen within this plain in between the ridges [48]. The coastal plain occupies a narrow strip of land that extends parallel to the Mediterranean Sea, with elevations ranging from 0 to 50 meters above sea level. The existence of alternating low-lying ridges separated by narrow depressions along the coast reflects the influence of lithologic and structural conditions as well as the fluctuation of sea level [23].

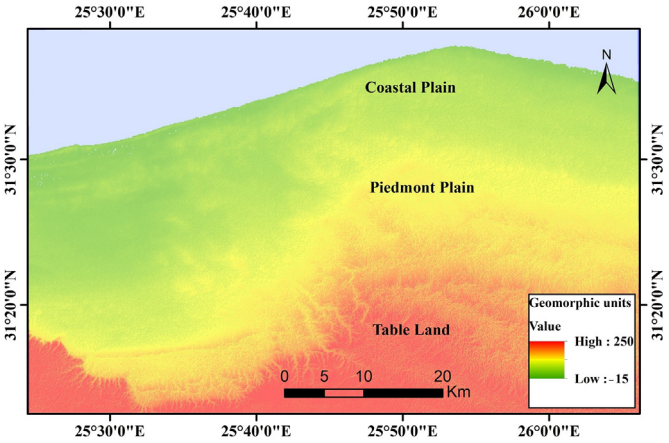

Figure 2. Geomorphological units.

Geologically, the study area, which is a part of the northwestern Mediterranean coast, is mainly underlain by sedimentary rocks ranging in age from Tertiary to Quaternary [23]. The Miocene deposits are represented by Moghra and Marmarica Formations. The Moghra Formation is composed of argillaceous limestone intercalated with sand and shale related to fluviatile to fluviomarine deposits, while the overlying shallow marine rocks belong to the Marmarica Formation. It is formed of fracture white limestone and a lower grey calcarenite interbedded with clay lenses. The overlaying Quaternary deposits are exposed in the study area. They are formed by a thin cover of drift sands and loamy deposits covering mainly low-lying areas and the floors of narrow valleys dissecting the tableland (Figure 3). The study area's climatic conditions are typically arid, with a long, hot, dry summer, a mild winter with little rainfall, high evaporation, and moderate to high relative humidity, with a mean annual rainfall of 155 mm [49].

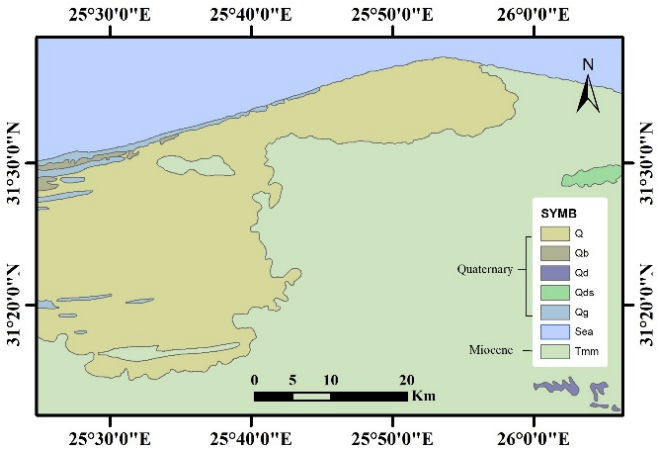

Figure 3. Surface geology map.

Hydrologically, the Quaternary and Miocene aquifers are considered as the two main water-bearing formations in the area under consideration. The Quaternary carbonate aquifer comprises wadi fill and oolitic limestone deposits, with a thickness ranging from 10 m to about 40 m [50,51]. It is mainly recharged from the infiltration of the precipitation over its outcropping rocks [50]. The Quaternary aquifer is directly connected to the Mediterranean Sea, which has a significant impact on groundwater salinity [51]. Groundwater, in this aquifer, exists under unconfined conditions and is represented by six groundwater samples. The depth to water ranges from 3.15 m (well 6) to 9.30 m (well 2), while the water level ranges between 2 m below sea level (well 1) and +4.7 m (well 3). The Miocene limestone aquifer of middle Miocene age (Marmarica Formation) is the main water-bearing formation

in the study area. It is mainly composed of successions of chalky, marly, argillaceous, and dolomitic limestones interbedded with clay lenses. The groundwater in this aquifer exists under two conditions: perched groundwater, where the water level is above mean sea level, and main water table, where the water is free or semi-confined. The perched water table is recharged indirectly by the overlying fractured rocks, while the fractured free to semi-confined aquifer is indirectly recharged by natural groundwater movement from south to north [51]. The degree of recharge depends on the nature of the fault from which this aquifer derives its water. The depth to water ranges from 16 m (well 11) to 72 m (well 41), whereas the water level ranges between 5.3 m below sea level (well 12) and +8 m (well 33). Despite the fact that there is a general relationship between water level and salinity because salinity frequently rises with the direction of water flow, Figure 4 shows that the relationship between the two variables is not clearly defined in each of the Quaternary and Miocene aquifers. This characteristic could mean that other hydrological factors, rather than the absolute water level, have a significant impact on the salinity of the water, as is the case in some localities within the study area, which showed perched aquifer conditions. In general, the figure shows a general direction of groundwater flow from southeast to northwest.

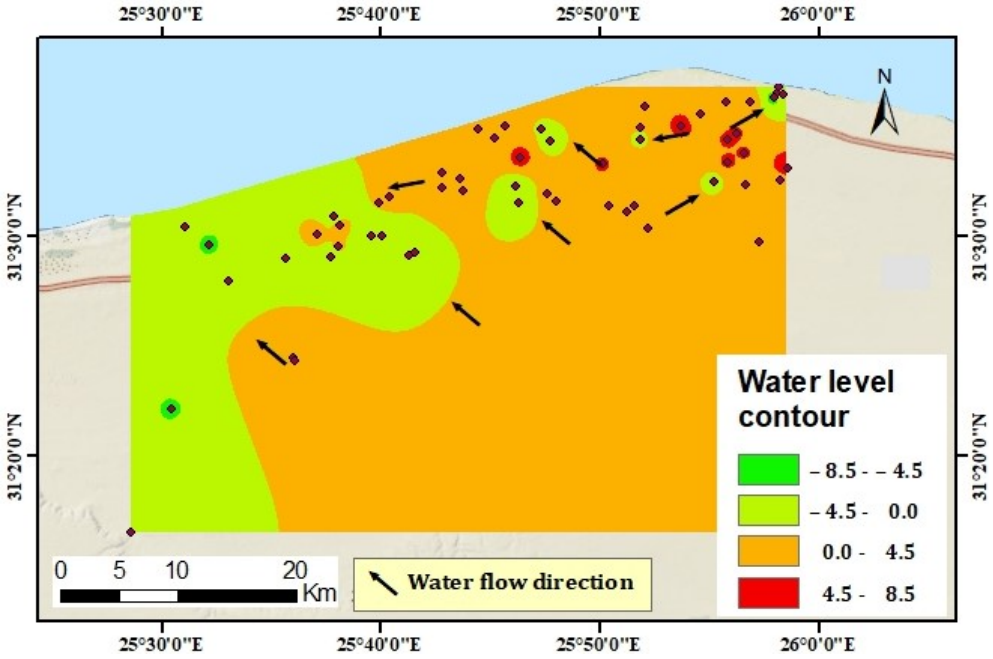

Figure 4. Water flow contour map. Points indicate sampling sites, while circles indicate areas with different water levels. The red circles represent the areas with the highest water level, while the green circles represent the areas with a low level of groundwater.

According to Morad et al. [51], the maximum discharge from the Quaternary and Miocene aquifers in the Barrani area is 52,200 m^3/day and 135,000 m^3/day, respectively. A hydrogeological cross-section extending from the southeast to the northwest towards the city of Baqbaq, with a distance of about 50 km (Figure 5), indicates that groundwater recharge is possible, with precipitation on the tablelands to the south and flowing to the Mediterranean Sea to the north. Because the karst aquifer's rocks are mostly fractured, recharge is possible and increasing along the drainage lines, where these drainage lines act as water collectors [52].

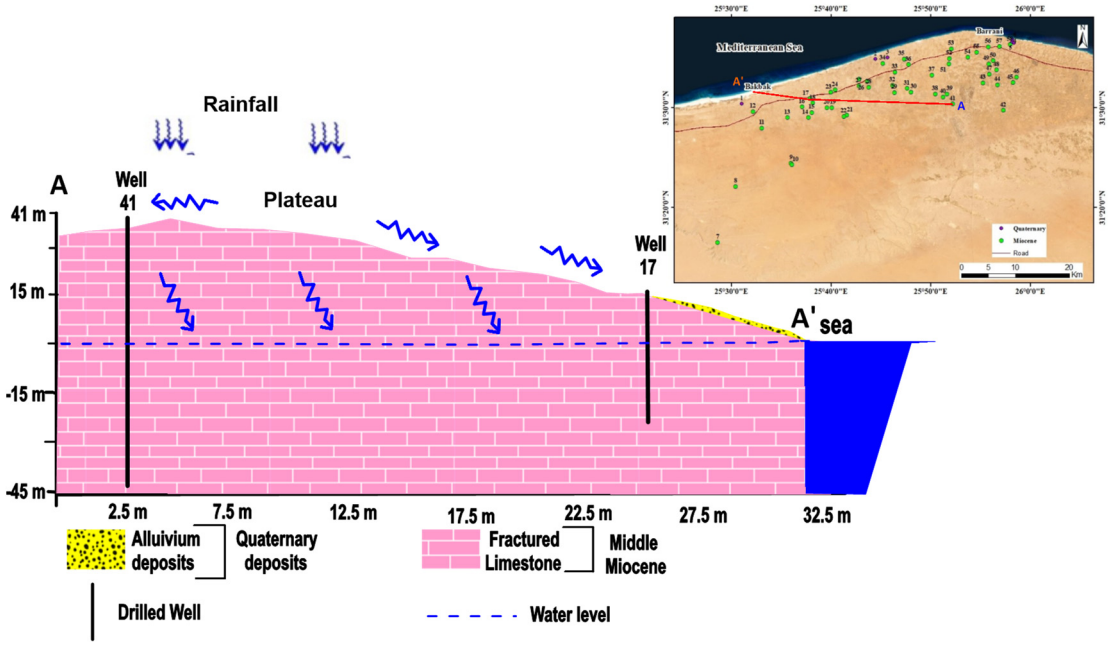

Figure 5. Hydrogeological cross section (A-A′), illustrating the karst aquifer subsurface succession and rainfall recharge opportunities.

4. Methodology

Fifty-eight groundwater samples were collected, throughout 2021, from all the available water points. These water points represent shallow hand dug and deep wells. The Quaternary aquifer was represented mostly by hand dug wells (6 samples), while the Miocene aquifer was primarily represented by drilled wells (52 samples). All the studied groundwater wells are private, with the exception of three governmental wells (12, 23, 44), which have desalination plants installed. Additionally, two water samples representing the local rainfall and the Mediterranean Sea were collected during the winter of 2020 to be used as reference waters. The rainwater sample (59) was collected from the rain gauge station located in the support center of the Desert Research Center in the Sidi Barani area, while the seawater sample (60) was collected from the Mediterranean Sea. The field activities included depth to water measurements and geographic locations of the wells, in addition to measuring the hydrogen ion activity (pH) and electrical conductivity (EC). During the field trip, only one water sample was collected from each well in order to perform the necessary chemical analyses. Another set of water samples was collected from selected wells for the purpose of conducting stable isotope analyses. The collected water samples were analyzed for major and minor ion concentrations (such as Ca, Mg, Na, CO_3, HCO_3, SO_4, Cl, SiO_2, and Br), in addition to environmental stable isotopes including $\delta^{18}O$ and $\delta^{2}H$. The concentrations of both CO_3 and HCO_3 were measured by the titration method using 0.01 normal H_2SO_4. The concentrations of the other major and minor ions were detected using ion chromatography (Dionex, ICS-1100, Thermo Fisher Scientific Inc., Waltham, MA, USA). All of the aforementioned analyses were conducted according to the methods adopted by Rainwater and Thatcher, Fishman and Friedman, and the American Society for Testing and Materials [53–55] at the Laboratory of the Desert Research Center, Egypt. The results of all of the analyzed water samples were within the acceptable error limit (±5).

The concentration of stable isotopes for some selected water samples were estimated according to the method described by Coplen et al. and Coplen [56,57] at the Center for Stable Isotopes at the University of New Mexico, USA. The results were reported in delta per mille (‰) notation for O-18 and deuterium (^{2}H) to identify the recharge sources as well as the factors affecting groundwater quality change. The assessment of the different hydrogeochemical and mixing processes were studied using multiple techniques, including the groundwater quality index for seawater intrusion (GQI_{SWI}), hydrochemical

facies evaluation diagram (HFE-D), ionic ratios and stable isotopes relationships, principle component analysis (PCA), and salinity mixing index (SMI) model. The software program Aquachem version 10 was used to identify the chemical water types, while ArcGIS desktop version 10.2 software, (Environmental Systems Research Institute, Inc. "ESRI", Redlands, CA, USA, was used to construct maps.

4.1. Gibbs Diagram

This diagram, a simple plot of the total dissolved solids (TDS) versus the weight ratio of Na/(Na + Ca) or Cl/(Cl + HCO_3), is used to identify the relationships between the chemical water composition and the types of the rocks in which the water circulates [58]. Three distinct fields, including precipitation dominance, evaporation dominance, and rock weathering dominance, constitute the segments in the Gibbs diagram.

4.2. Hydrochemical Facies Evolution Diagram (HFE-D)

This diagram was suggested by Gimenez Forcada [59] as an alternative to other hydrochemical diagrams such as the piper diagram, to clearly identify the hydrogeochemical changes in groundwater during recharge and saltwater intrusion processes. The importance of this diagram is that it helps in the identification of the salinization–freshening phases in coastal aquifers. In addition, it contributes to a clearer identification of possible groups of samples and their evolution trends in the aquifer [60,61]. In this diagram, four main facies are defined, namely NaCl, $CaCl_2$, $NaHCO_3$, and $CaHCO_3$. Each group is divided in turn into four other subfacies, resulting in sixteen subdivisions. These subdivisions are the following: 1. Na–HCO_3/SO_4, 2. Na–MixHCO_3/MixSO_4, 3. Na–MixCl, 4. Na–Cl, 5. MixNa–HCO_3/SO_4, 6. MixNa–MixHCO_3/MixSO_4, 7. MixNa–MixCl, 8. MixNa– Cl, 9. MixCa–HCO_3/SO_4, 10. MixCa–MixHCO_3/MixSO_4, 11. MixCa–MixCl, 12. MixCa–Cl, 13. Ca–HCO_3/SO_4, 14. Ca–MixHCO_3/MixSO_4, 15. Ca–MixCl, 16. Ca–Cl [62]. The facies in this diagram are determined by the percentage of Ca and Na cations, as well as by HCO_3 (or SO_4) and Cl^- anions, in relation to the sum of cations and anions. The term Mix is used for the facies names to indicate that the percentage of the cations or anions is less than 50% but greater than the percentage of any of the other cations and anions considered. For example, if a sample is plotted in subdivision 6, it belongs to MixNa–MixHCO_3/MixSO_4, which means none of the Na, HCO_3, and SO_4 ions reached 50%, yet Na% remains greater than Ca and Mg, and similarly, HCO_3 and SO_4 will be greater than Cl. In addition to the mixing processes, the diagram also explains both the direct and reverse exchange reactions.

4.3. Correlation Coefficients (Ion–Ion Relationships)

Changes in the chemical composition of groundwater are affected by many factors, such as rock–water interaction, mixing, and ion-exchange processes. Some parameters and ion ratios calculated in meq/L (such as Ca_{excess}, $Na_{deficit}$, Na/Cl, Mg/Ca, SO_4/Cl, and Br/Cl) are addressed. They were correlated with each other as well as with the TDS in bivariate diagrams in order to distinguish between the mixing mechanisms of fresh water and saline water from other chemical reactions, such as rock weathering and ion exchange.

4.4. Principal Component Analysis (PCA)

Principal component analysis (PCA) is a data transformation technique that attempts to visualize a simple underlying structure that is assumed to exist within a multivariate data set [63]. It quantifies the relationship between different variables by computing the correlation matrix for the entire data set. As a result, the data set is easily summarized without losing much information [64]. When using this technique, data sets are first standardized, and then the correlation matrix is created. The eigenvalues and factor loadings for the correlation matrix are determined and a scree plot is drawn. The extraction factors are based on the variances and co-variances of the variables. The eigenvalues and eigenvectors are evaluated, which represent the amount of variance explained by each factor. An eigenvalue greater than 1 is set as a criterion to extract factors [65]. Finally, by the

process of rotation, the loading of each variable on one of the extracted factors is maximized, and the loadings of all the other factors are minimized. These factor loadings are useful in grouping the water quality parameters and providing information for interpreting the data. This study considered pH, EC, Na, K Ca, Mg, Cl, CO_3, HCO_3, and SO_4 as water quality parameters. Statistical Package for the Social Sciences (SPSS) version 16 was used for the statistical analysis.

4.5. Groundwater Quality Index for Seawater Intrusion (GQI_{SWI})

The GQI_{SWI} index was developed by Tomaszkiewicz et al. [66] as another tool, calculated according to Piper [67], to interpret groundwater quality change (in terms of seawater salinization). Equation (1) is developed from Equations (2)–(4):

$$GQI_{SWI} = \frac{GQI_{Piper\ (mix)} + GQI_{fsea}}{2} \quad (1)$$

$$GQI_{Piper\ (mix)} = \left(Ca^{2+} + Mg^{2+} + HCO_3^-\right) \times 50\ (in\ \%\ meq/l) \quad (2)$$

$$GQI_{fsea} = (1 - f_{sea}) \times 100 \quad (3)$$

where

$GQI_{Piper\ (mix)}$ is the freshwater seawater mixing index of the piper diagram;
GQI_{fsea} is seawater fraction index.
The seawater fraction (f_{sea}) is calculated according to the following equation:

$$f_{sea} = \frac{m_{Cl\ sample} - m_{Cl\ fresh}}{m_{Cl\ sea} - m_{Cl\ fresh}} \quad (4)$$

Chloride ion is used as a conservative parameter, where $m_{Cl\ sea} - m_{Cl\ fresh}$ is equal to about 35‰ (grams of salt per kilogram) seawater, based on the concentration of Cl^- in mmol/L [66,68]. GQISW is a numerical indicator used to interpret data from the Piper diagram as well as seawater intrusion. It ranges from 0 to 100, with 100 representing freshwater and 0 representing seawater.

4.6. Seawater Mixing Index (SMI)

The seawater mixing index (*SMI*) is applied to calculate the degree of seawater mixing [69]. Major ion compositions, including (Cl, SO_4, Na and Mg), are used to calculate this index according to the following equation:

$$SMI = a \times \frac{C_{Na}}{T_{Na}} + b \times \frac{C_{Mg}}{T_{Mg}} + c \times \frac{C_{Cl}}{T_{Cl}} + d \times \frac{C_{SO_4}}{T_{SO_4}} \quad (5)$$

The constants a, b, c, and d are estimated based on the relative concentration proportion of Na^+, Cl^-, Mg^{2+}, and $SO_4{}^{2-}$ in seawater and recorded as 0.31, 0.04, 0.57, and 0.08, respectively. C is the measured ion concentration in mg/L. T represents the values of threshold of the selected ions, which can be estimated from the cumulative probability curves by determining the inflection points for each ion. The water is said to be impacted by seawater mixing if the *SMI* is more than 1 [70].

5. Results and Discussion

Groundwater characterization mainly depends on its chemical constituents. The concentrations of these constituents are mostly a result of the interaction between groundwater and its host rocks. In this part, different aspects are addressed, including hydrochemical characterization, salinization process identification, and mixing ratio quantification.

5.1. Hydrochemistry and Its Prevailing Factors

The physical, chemical, and isotopic characteristics of groundwater samples from the shallow Quaternary (samples 1 to 6) and deeper Miocene (samples 7 to 58) wells are presented in Table 1 and Figure 6. The total dissolved solids (TDS) displayed high variance, ranging from 1113 mg/L to 51,975 mg/L (Avg. 10,290 mg/L). The high values and extreme outliers in TDS values are probably due to salt water. The major cations followed the order Na (260–15,000 mg/L, Avg., 2738 mg/L) > Mg (46–2292 mg/L, Avg., 500 mg/L), or Ca (47–1887 mg/L, Avg. 423 mg/L), while the major anions are of the order Cl (406–29,200 mg/L, Avg., 4786 mg/L) > SO_4 (200–4300 mg/L, Avg., 1778 mg/L) > HCO_3 (49–460 mg/L, Avg., 174), indicating that groundwater is dominated by two hydrochemical types: Na-Cl and Na-SO_4. Groundwater samples collected from the Quaternary and Miocene aquifers were classified into four groups according to USGS [71]. Group A, which is classified as slightly saline water (5 samples, and its percentage is 9%), ranged from 1000 to less than 3000 mg/L. Group B (26 samples, about 45%), with salinity ranging from 3000 to 10,000 mg/L, is classified as moderately saline water. Group C (25 samples of about 43%), whose salinity ranged from 10,000 to 35,000 mg/L, is classified as highly saline water. Finally, group D, with a very high salinity (more than 35,000 mg/L), is represented by two samples of about 3%. The majority of the studied groundwater samples, which mainly belong to the Miocene aquifer, are represented by Group B and C, while almost all the Quaternary samples belong to Group D. The hydrogen ion activity (pH) values reveal that groundwaters are neutral to slightly alkaline, with a mean pH value of 7.18. The water type shown in Table 1 is mainly characterized as a Cl–Na type, except two samples are of Cl-SO_4-Na type, indicating advanced evolutionary stages of groundwater.

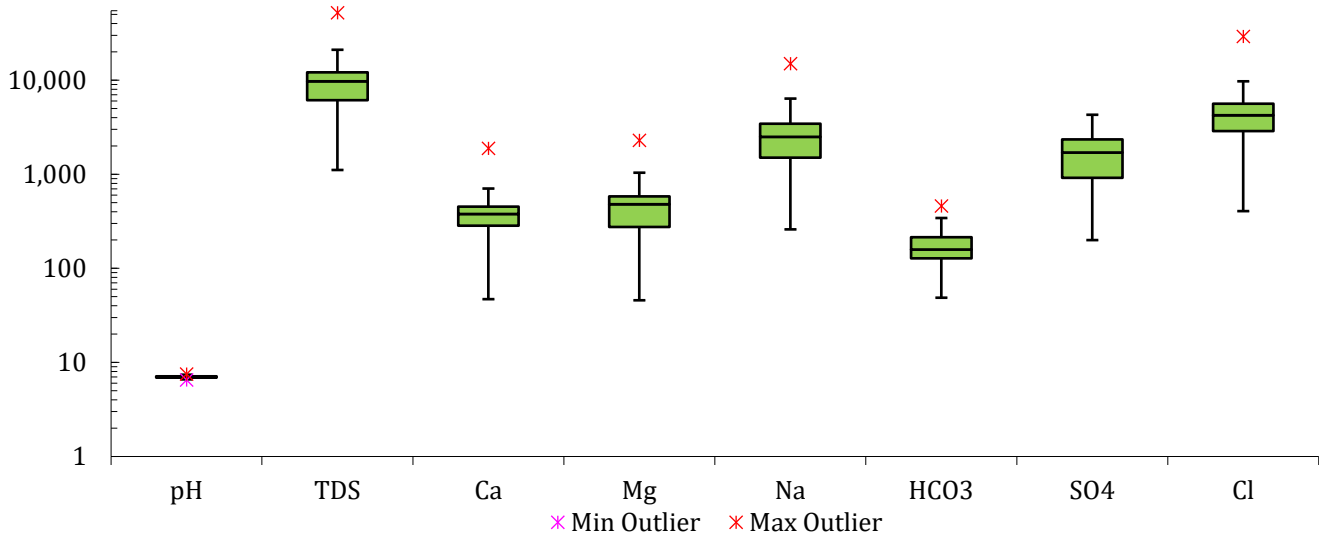

Figure 6. Box plot showing the distribution of the major cations and anions for the studied groundwater samples.

Table 1. Chemical and isotopic data of the sampled wells.

Aquifer	Well	EC (µs/cm)	pH	TDS mg/L	Water Level	Water Type	Cations (mg/L)				Anions (mg/L)				SiO_2 mg/L	Br mg/L	$\delta^{18}O$‰	δD‰
							Ca	Mg	Na	K	CO_3	HCO_3	SO_4	Cl				
Quaternary	1	95,400	6.8	51,975	−2	Na-Cl	1886.79	2292.45	15,000	35	18	85.4	3500	29,200.00	20.33	29.50	0.26	1.40
	2	25,380	17	13,589	0.7	Na-Cl	603.77	550.19	3700	67	6	115.9	2000	6603.77	12.98	6.60	−3.82	−21.80
	3	12,420	7.1	5315	4.7	Na-Cl	226.42	412.64	1100	60	6	359.9	500	2830.19	17.11	3.66	–	–
	4	21,820	6.9	11,178	−1	Na-Cl	127.7	239.8	3500	87	12	286.7	3200	3867.92	13.40	7.55	−4.39	−19.50
	5	28,450	7	16,854	0	Na-Cl	371.3	412.6	5000	90	12	128.1	4300	6603.77	19.80	9.45	–	–
	6	30,600	7	17,420	−2.15	Na-Cl	220.7	339.0	5500	200	21	128.1	4000	7075.47	11.32	10.70	–	–
Miocene	**7**	2711	7.3	1217	−2	Na-Cl	75.47	74.50	260	10	6	237.9	200	471.70	33.44	0.63	−6.38	−33.25
	8	10,920	7.1	5306	−4.75	Na-Cl	207.55	171.93	1350	148	0	140.3	1330	2028.30	33.74	2.77	−5.34	−31.20
	9	6750	7.3	3696	3.5	Na-Cl	188.68	91.70	980	22	12	256.2	1000	1273.05	42.36	2.25	−5.56	−28.70
	10	5170	7.4	3013	3.5	Na-Cl	113.21	126.08	740	43	6	134.2	880	1037.30	19.77	1.63	–	–
	11	68,500	6.7	37,548	−1	Na-Cl	1886.79	1833.96	10,000	24	24	158.6	2900	20,800.00	13.94	22.40	–	–
	12	30,400	6.9	16,249	−5.3	Na-Cl	377.36	550.19	5000	100	6	48.8	1700	8490.57	4.97	8.52	0.62	5.10
	13	8670	7.2	5148	−2	Na-Cl	230.00	320.00	1050	40	6	219.6	1600	1792.45	14.30	2.41	−5.17	−28.36
	14	21,290	7	10,006	−4	Na-Cl	374.40	581.26	2600	77	31.2	126.88	700	5578.70	28.20	1.68	–	–
	15	23,250	7	12,042	0.75	Na-Cl	264.15	550.19	3300	82	9	140.3	2200	5566.04	15.51	6.63	−4.62	−27.40
	16	29,340	7	14,509	2	Na-Cl	452.83	550.19	4000	110	9	195.2	2120	7169.81	25.85	10.20	–	–
	17	25,880	7	14,131	−4	Na-Cl	377.36	596.04	3700	91	30	103.7	3200	6084.91	18.15	8.69	–	–
	18	31,300	6.9	14,585	2	Na-Cl	450.00	800.00	3600	106	6	146.4	2050	7500.00	14.04	8.91	−4.19	−25.50
	19	9800	7.1	55,80	−2.3	Na-Cl	301.89	183.40	1500	33	18	158.6	540	2924.53	23.06	3.22	–	–
	20	4590	7.4	2126	−23	Na-Cl	108.16	111.20	500	29	23.4	261.69	220	1003.19	13.23	3.24	−6.30	−35.30
	21	4460	7.4	2044	−2.3	Na-Cl	47.17	85.97	560	26	6	225.7	440	766.51	18.04	1.33	–	–
	22	2388	7.5	1395	0.4	Na-Cl	96.00	75.00	280	14	6	195.2	390	436.32	16.16	0.72	−6.65	−33.61
	23	31,400	6.8	16,793	–	Na-Cl	452.83	916.98	4200	67	18	128.1	3150	7924.53	22.81	9.37	−4.31	−24.60
	24	16,720	7.3	9389	1.5	Na-Cl	452.83	275.09	2600	50	12	146.4	1020	4905.66	29.57	5.28	–	–
	25	15,180	7.1	8553	1.25	Na-Cl	452.83	366.79	2000	46	18	91.5	1850	3773.58	14.40	4.64	–	–
	26	14,730	7.1	7836	2	Na-Cl	377.36	275.09	2150	38	12	115.9	680	4245.28	37.34	4.41	–	–
	27	16,630	7	8999	0.5	Na-Cl	603.77	320.94	2200	35	18	158.6	2440	3301.89	25.72	3.60	–	–
	28	13,170	7.1	6870	1	Na-Cl	452.83	275.09	1600	35	18	140.3	1400	3018.87	17.22	3.83	−4.62	−27.00
	29	20,410	7	10,436	−5	Na-Cl	332.80	833.98	2300	53	7.8	222.04	2100	4697.86	38.60	5.26	−4.28	−24.30
	30	20,870	7	10,582	3	Na-Cl	624.00	505.44	2500	51	7.8	459.94	2260	4404.24	38.71	5.86	–	–
	31	28,400	6.8	14,015	0.5	Na-Cl	665.60	808.70	3400	61	7.8	237.9	2200	6753.17	23.04	8.00	−4.19	−24.50
	32	19,310	6.8	11,140	−4	Na-Cl	374.40	581.26	2600	57	15.6	166.53	3220	4208.50	38.79	5.06	–	–
	33	19,540	6.6	9470	8	Na-Cl	332.80	505.44	2300	61	7.8	222.04	1650	4502.11	17.37	5.55	–	–
	34	17,820	6.9	9722	0.8	Na-Cl	377.36	366.79	2700	30	0	170.8	2200	3962.26	15.15	4.92	–	–
	35	17,030	6.9	10,565	−0.5	Na-Cl	301.89	504.34	2800	60	12	427	2900	3773.58	16.39	4.56	–	–
	36	10,740	7.1	5879	−3	Na-SO4	264.15	298.02	1300	37	12	176.9	2700	1179.25	13.88	3.05	−4.95	−25.50
	37	26,060	6.9	14,136	5.2	Na-Cl	540.80	808.70	3500	74	7.8	182.39	2850	6263.81	21.36	–	−4.38	−23.40
	38	18,740	7.1	10,445	4	Na-Cl	332.80	606.53	2600	33	7.8	214.11	2060	4697.86	20.30	4.82	−4.60	−26.20
	39	13,170	7	8144	3.1	Na-Cl	478.40	694.98	1470	54	15.6	111.02	1950	3425.52	27.39	5.88	–	–
	40	11,940	7.1	6569	4	Na-Cl	291.20	454.90	1500	33	7.8	214.11	750	3425.52	18.21	3.82	–	–
	41	15,550	7	7507	2	Na-Cl	395.20	518.08	1700	22	7.8	142.74	780	4012.75	14.26	4.22	−5.17	−31.00
	42	12,350	7.1	6396	2	Na-Cl	452.83	412.64	1300	33	6	122	1300	2830.19	15.00	3.45	−5.31	−32.20
	43	19,980	7.1	9958	−3	Na-Cl	374.40	505.44	2500	31	7.8	150.67	2060	4404.24	14.60	5.10	–	–
	44	20,150	7	12,520	2	Na-Cl	452.83	458.49	3400	62	0	103.7	3000	5094.34	13.02	5.50	−1.42	−9.20
	45	1872	7.1	1113	1	Na-Cl	60.38	45.85	270	7	6	115.9	260	405.66	10.52	0.75	–	–
	46	11,460	7	6884	9	Na-Cl	301.89	137.55	2000	35	6	146.4	1500	2830.19	13.02	3.27	–	–
	47	19,580	6.9	8197	5.4	Na-Cl	224.0	231.7	2600	61	12	91.5	400	4622.64	13.00	4.49	−4.57	−23.30

Table 1. *Cont.*

Aquifer	Well	EC (µs/cm)	pH	TDS mg/L	Water Level	Water Type	Cations (mg/L)				Anions (mg/L)				SiO_2 mg/L	Br mg/L	$\delta^{18}O$‰	δD‰
							Ca	Mg	Na	K	CO_3	HCO_3	SO_4	Cl				
	48	15,070	6.5	6905	4.8	Na-Cl	206.2	212.5	2000	55	6	158.6	950	3396.23	15.58	4.09	–	–
	49	20,850	6.9	11,705	5	Na-Cl	247.3	319.5	3600	61	6	131.15	2500	4905.66	14.31	6.26	–	–
	50	20,850	6.9	11,160	5	Na-Cl	240.4	331.2	3300	70	12	91.5	1500	5660.38	13.42	4.47	–	–
	51	25,210	6.8	14,890	−1	Na-Cl	452.83	687.74	3900	50	6	122	3600	6132.08	19.29	6.94	–	–
	52	23,230	6.9	10,649	0	Na-Cl	377.36	504.34	2900	75	6	183	1600	5094.34	18.28	6.86	–	–
	53	22,520	6.7	10,617	1	Na-Cl	528.30	458.49	2800	51	0	158.6	1700	5000.00	13.18	6.21	−4.35	−22.10
	54	20,220	6.9	12,178	7	Na-Cl	528.30	412.64	3500	36	0	115.9	1700	5943.40	14.08	5.41	–	–
	55	11,430	7.2	6564	1	Na-Cl	250.1	157.0	1900	50	15	146.4	1100	3018.87	14.05	3.06	–	–
	56	15,060	6.9	5631	4	Na-Cl	231.4	226.9	1500	60	6	210.45	200	3301.89	16.08	4.68	–	–
	57	8790	7.1	5319	3.8	Na-Cl-SO4	106.1	145.6	1500	42	18	213.5	1750	1650.94	12.90	2.63	–	–
	58	8240	7.1	4148	1	Na-Cl	126.0	111.7	1200	37	6	237.9	850	1698.11	16.26	2.95	–	–
Rain	59	120	8.73	74	–	Na-HCO3	8.00	3.50	15.1	2	2.6	47.45	13	6.40	0.00	0.45	−3.85	−13.98
Sea	60	59,300	7.71	36,226	–	Na-Cl	518.00	1441.00	10,210	371	24	148	3129	20,459.00	0.62	298.00	1.34	9.58

(–) not measured.

5.2. Groundwater Salinization and Mixing Processes

Different geochemical mechanisms, including rock–water interaction, evaporation, and precipitation, were identified when water samples were plotted on Gibbs diagrams (Figure 7). It is clearly shown on these diagrams that the water chemistry of almost all the Quaternary and Miocene groundwater samples is mainly controlled by evaporation-precipitation processes and seawater intrusion, plotted in the upper right corner of the diagram. It is also apparent that most of the samples with Na/(Na + Ca) or Cl/(Cl + HCO_3) ratios greater than 0.6 and TDS values greater than 5000 mg/L were mainly affected by saline water mixing or evaporation. This plot showed also that few samples were located in the rock dominance region, indicating that rock–water interaction has little impact on groundwater chemistry.

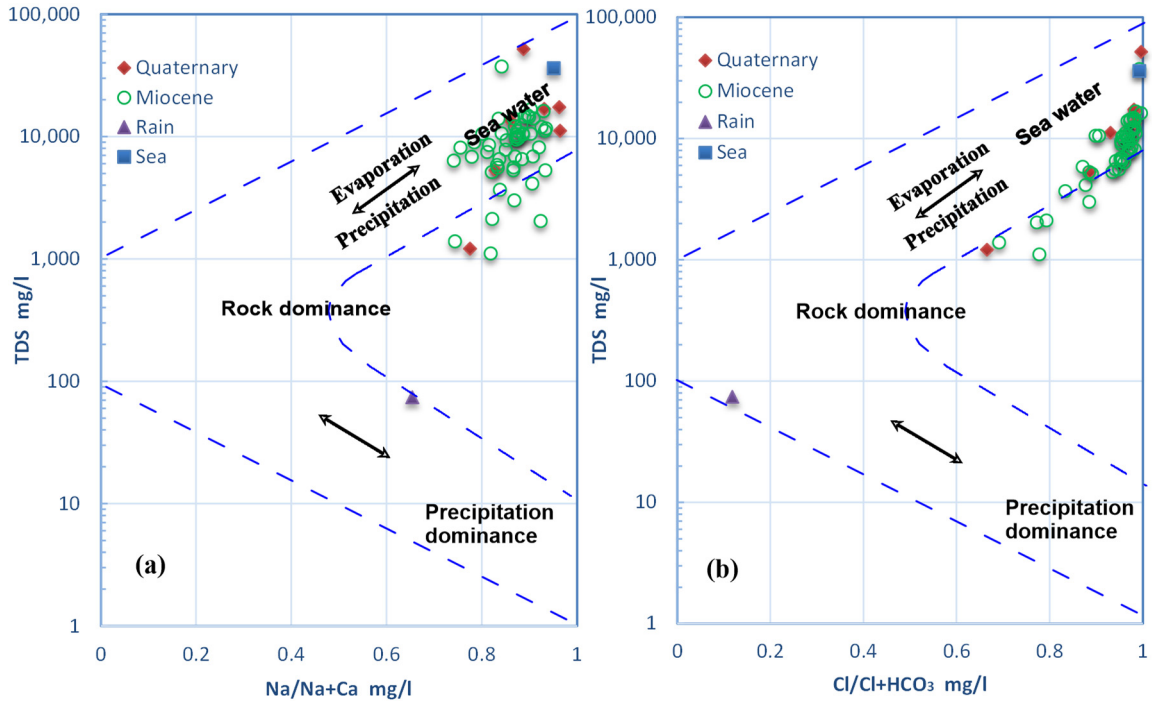

Figure 7. Gibbs diagrams showing TDS versus (**a**) Na/(Na + Ca) and (**b**) Cl/(Cl + HCO_3).

Groundwater samples were plotted in the Hydrochemical Facies Evolution Diagram (HFE-D); seawater and freshwater were connected through a mixing line (Figure 8). It is shown that the dominant water facies type is Na-Cl, where almost all samples were plotted in subdivision 4, and only two samples are of Mix/Na-Cl, located in subdivision 8. This means that Na ions exceed 50% of the total percent of cations as is also the case with respect to Cl ions. Samples can be divided into two groups. The first group is located below and to the right of the seawater/freshwater mixing line, indicating seawater/saltwater intrusion. The other group is situated down to the left of the line. While it still has the same facies, it is somewhat affected by recharge from fresh water. This diagram also indicates that a group of samples were subjected to direct cation exchange, with Na ions being released to the solution, while other samples were affected by an inverse cation exchange reaction. Delineation of the salinization processes in the study area will be more clearly elucidated in the following sections.

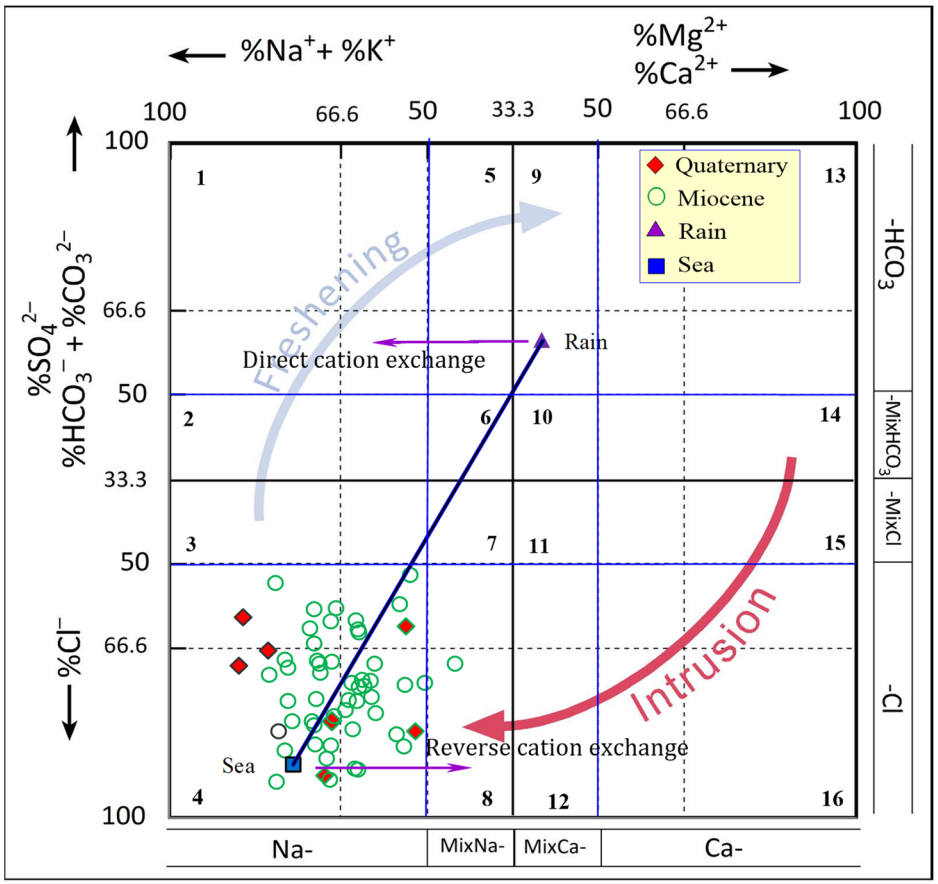

Figure 8. Hydrochemical facies evaluation diagram (HEF-D).

5.2.1. Ion Ratios and Correlation Coefficients

Ionic chemical ratios are useful for the identification of different hydrochemical processes affecting water quality as well as the impact of seawater intrusion on groundwater chemistry [72,73]. The ion ratios selected are summarized in Table 2.

Table 2. Ranges and average values of some ratios of the studied groundwater samples.

Ratio	Na/Cl	Mg/Ca	SO_4/Cl	Br/Cl
Quaternary aquifer				
Range	0.60–1.4	1.5–3.1	0.09–0.61	0.0044–0.0087
Average	1.00	2.33	0.33	0.0061
Miocene aquifer				
Range	0.65–1.7	0.75–4.13	0.04–1.69	0.0013–0.0143
Average	0.92	1.95	0.36	0.0058
Rain	3.64	0.72	1.5	0.0312
Sea	0.77	4.59	0.11	0.0065

The Na/Cl ratio is less than unity in the majority of the Miocene samples and in half of the Quaternary samples, while the rest of the samples showed values greater than unity. The relationship between Cl and Na/Cl (Figure 9A) showed that many samples plot on the 1:1 line, indicating the role of halite dissolution as a major process contributing to groundwater salinization [68]. A few samples showed slight increases in sodium relative to chloride, reflecting the effect of recharge from rainwater and/or ion exchange. The majority of samples plot slightly below that line, with a higher chloride content compared to sodium, indicating the probability of seawater intrusion.

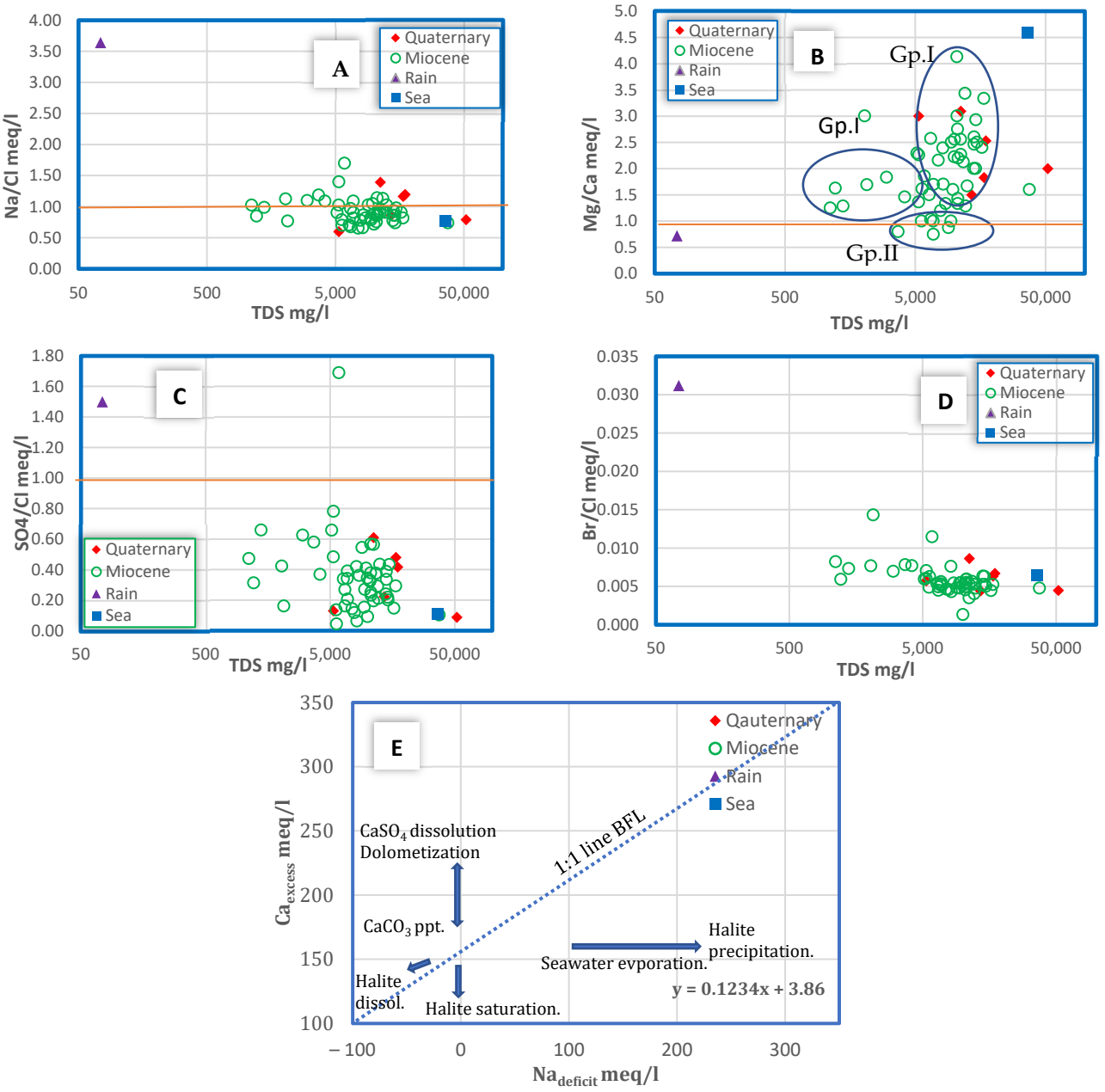

Figure 9. (**A**–**D**) Bivariate plots of some ion ratios vs. TDS; (**E**) $Na_{deficit}$ meq/L vs. Ca_{excess} meq/L plot.

The Mg/Ca ratio is used to interpret the impact of the aquifer matrix dominated by carbonate rocks as well as the effect of seawater on groundwater; it tends to be 1 in freshwater and approaches 5 in seawater [74,75]. In Figure 9B, there are three groups. The first is a group with slightly lower salinity (less than or equal 5000 mg/L) and a higher value of Mg/Ca, reflecting cation exchange and recharge from freshwater. The second group, which represents the majority of samples, has higher values of TDS as well as Mg/Ca. This group is mainly affected by marine rock–water interaction and seawater intrusion processes. The third group, with lower Mg/Ca and relatively higher Cl content, indicates a long residence time in carbonate rocks and recharge from fresh water. The SO_4/Cl ratio is considered as evidence of the influence of marine deposits as well as seawater on groundwater, with values below unity in almost all samples (Figure 9C). As Br and Cl are relatively conservative in hydrological systems, the Br/Cl ratio is used to distinguish whether groundwater salinity is of marine or non-marine origins [76]. As shown in both Table 2 and Figure 9D, the Br/Cl ratios of most of the studied groundwater samples are

within the normal seawater range (0.0040–0.0070) as salinity increases, with a mean value of about 0.006, indicating that the salinization of these groundwaters resulted from dissolution of marine sediments and mixing with seawater.

The slight decrease of the Br/Cl ratio with higher salinity is likely due to interaction with rocks rich in evaporites. On the other hand, samples with relatively low salinity but with a higher Br/Cl ratio suggest the impact of anthropogenic activities on groundwaters [77]. This could be explained as a result of the impact of the on-site wastewater disposal on groundwater, as some residents resort to using abandoned wells for sewage in the area under consideration. The relationship between $Na_{deficit}$ and Ca_{excess} in basinal fluids is presented according to Davisson et al. and Davisson and Criss [78,79] using two parameters:

$$Ca_{excess} = 2[Ca_{meas} - (Ca/Cl)_{SW} \times Cl_{meas}]/40.08 \quad (6)$$

$$Na_{deficit} = [(Na/Cl)_{SW} \times Cl_{meas} - Na_{meas}]/22.99 \quad (7)$$

A straight $Na_{deficit}$ Ca_{excess} regression line with a 1:1 slope, known as the Basinal Fluid Line (BFL; [79]), is plotted for the majority of basinal brines in the world, showing water–rock interaction with a net cation exchange ratio of 1 Ca for 2 Na (Figure 9E). This diagram shows the various chemical processes that the groundwater has undergone. Such processes include (i) halite dissolution with a trend that extends from the origin (0,0 point) towards the negative quadrant of the plot; (ii) cation exchange for the samples plotted on the 1:1 line; and (iii) seawater evaporation after calcite precipitation following a nearly horizontal trend, with a slope of 0.123. Further evaporation with a decrease in Na concentration will result in the precipitation of halite, as indicated by the samples plotted slightly above the seawater sample.

5.2.2. Saturation Indices

PHREEQC version 3 [80] calculated saturation indices by comparing the chemical activities of the mineral's dissolved ions (ion activity product, IAP) with their solubility product (Ksp). The saturation indices (SI) for selected minerals, including anhydrite, calcite, dolomite, gypsum, and halite, were calculated to confirm the precipitation and dissolution of these minerals. They have negative values when the minerals tend to dissolve, positive values when the minerals tend to precipitate, and zero values when the water and minerals are in chemical equilibrium. The minerals chosen were based on the major ions encountered in the study area's groundwater. Figure 10 depicts a bivariate diagram of SI values for anhydrite, calcite, dolomite, gypsum, and halite against the chloride concentration of the studied groundwater samples. It shows a positive correlation between Cl concentration and SI values. The plot shows that groundwater samples are undersaturated with respect to calcite and dolomite, with 78% and 40%, respectively. All samples exhibited undersaturation in relation to anhydrite, gypsum, and halite. The positive values of the calculated SI with respect to calcite and dolomite were about 22% and 60%, respectively, and the negative values of SI for all groundwater samples with respect to anhydrite and gypsum suggest that these salts have a major role in the enrichment of groundwater with calcium and sulphate.

This figure also shows that there are three groups; group I, with intermediate Cl concentration; group II, with a higher Cl concentration; group III, with much higher Cl concentration, which reached or exceeded the seawater values (as in samples 1 and 11). Group I is plotted near the midway between the recharge water (rainwater) and the seawater, indicating the leaching and dissolution of marine sediments. gp II is closely plotted next to seawater, reflecting mixing with seawater as a result of groundwater overexploitation and scarcity of recharge from precipitation. Finally, gp III includes seawater and samples subjected to the dissolution of salt marches rich in evaporates.

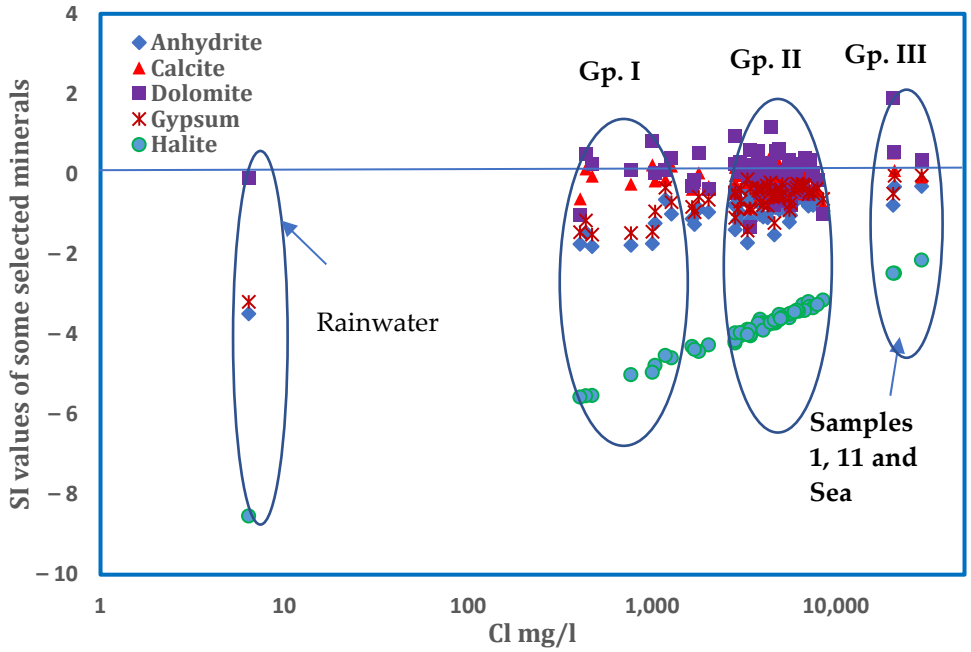

Figure 10. Relationship between Cl in mg/L and saturation indices for selected minerals.

5.2.3. Stable Isotopes

Environmental stable isotopes such as Oxygen-18 and deuterium are good indicators for tracing the recharge sources and the origin of groundwaters, as they do not participate in geochemical reactions except in geothermal systems. Isotope exchange usually takes place within geothermal water systems only at elevated temperatures (>250 °C) [81]. The stable isotopic compositions of the collected water samples are listed in Table 1. The isotopic content of the Quaternary samples ranged from −4.39 to 0.26‰ (Avg. −2.65) for $\delta^{18}O$; from −21.80‰ to 1.40‰ (Avg. −13.30) for deuterium. For the Middle Miocene aquifer, $\delta^{18}O$ values ranged from −6.65‰ to 2.60‰ (Avg. −4.56‰) and ranged between −35.30‰ and 5.10‰ (Avg. −25.31‰) for deuterium. The plot of $\delta^{18}O$ versus δD for the studied groundwater samples is shown in Figure 11a. The global meteoric water line GMWL [82], described by the equation $\delta D = 8\ \delta^{18}O + 10‰$, and the corresponding line for Mediterranean precipitation MMWL [83], described by the equation $\delta D = 8\ \delta^{18}O + 22‰$, are shown as references. It is shown that most of the groundwater samples plot very close to the Mediterranean meteoric water line (MMWL), indicating recharge from Mediterranean precipitation. According to Olive [84], if there is mixing between the coastal groundwater and seawater, the water samples will plot on a mixing line (ML) with the equation $\delta D = 5.5\ \delta^{18}O + 0.0‰$.

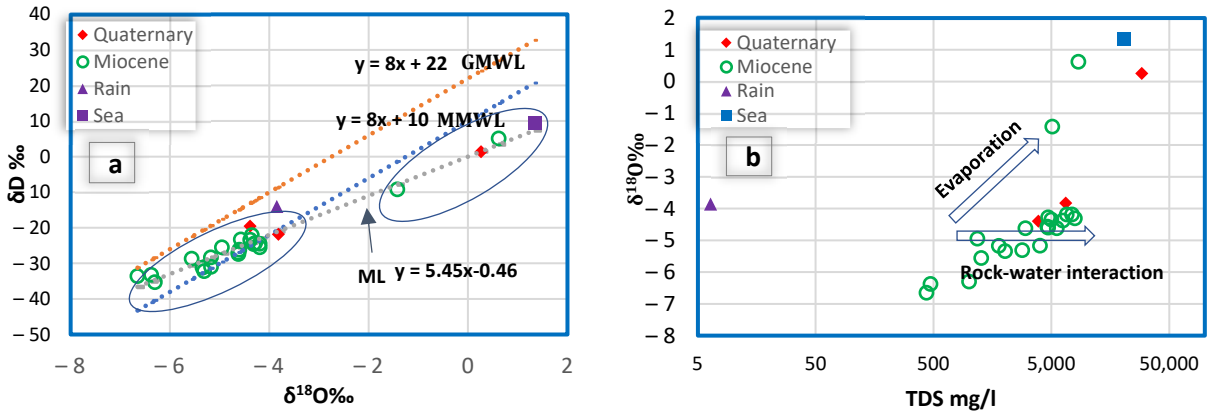

Figure 11. (**a**) $\delta^{18}O‰$ vs. δD; (**b**) TDS vs. $\delta^{18}O‰$.

The distinctive trend expressing the mixing of groundwater with more evaporated water (seawater) is represented by the mixing line (ML) (Figure 11a). This line is described by the equation $\delta D = 5.45\ \delta^{18}O - 0.46‰$, which is similar to the equation proposed by Olive [84]. It is shown that almost all groundwater samples were situated on that line and can be divided into two groups. First is the group with depleted isotope values, indicating that it is of meteoric origin. The other group, with more enriched in $\delta^{18}O$ and δD values, is assumed to have been exposed to mixing with seawater and/or the fractionation during evaporation from the shallow groundwater aquifers. The purpose of using the relationship between TDS and $\delta^{18}O$ is to distinguish between samples that were exposed to evaporation from those that were subjected to leaching and dissolution. It is noted from Figure 11b that the majority of groundwater samples, characterized by relatively high salinity, were mainly subjected to leaching and dissolution of marine deposits. The remaining group of samples, of much higher salinity, was affected by dissolution of evaporites (such as halite, anhydrite, and/or gypsum).

5.2.4. Principle Component Analysis (PCA)

Principle component analysis was applied to identify relationships between different variables, including pH, TDS, Ca, Mg, Na, K, CO_3, HCO_3, SO_4, Cl, $\delta^{18}O$, δD, SMI, and GQI_{SWI}, and to extract different factors affecting groundwater quality (Tables 3 and 4). The correlations established between the selected parameters (Table 3) show that there is a strong correlation between TDS and the concentrations of the variables Ca, Mg, Na, SO_4, Cl, Br, $\delta^{18}O$, δD, and SMI ($r^2 \geq 0.7$), indicating that such variables are enriched due to mineralization processes. The high correlation between TDS and both $\delta^{18}O$ and δD is evidence of the exposure of groundwater to evapoconcentration processes. Although the aquifer matrix is dominated by carbonate rocks, bicarbonates are not correlated with calcium, indicating a source other than calcite dissolution. Meanwhile, calcium is well correlated with SO_4 ($r^2 \geq 0.53$), suggesting gypsum dissolution. The factor loadings of the correlation matrix were defined based on eigenvalues that exceeded unity [65].

Table 3. Correlation matrix for selected parameters.

Variable	pH	TDS	Ca	Mg	Na	K	CO_3	HCO_3	SO_4	Cl	Br	SiO_2	$\delta^{18}O$	δD	SMI	GQI_{SWI}
pH	1.00															
TDS	0.00	1.00														
Ca	0.07	0.94	1.00													
Mg	−0.04	0.95	0.93	1.00												
Na	0.01	1.00	0.92	0.92	1.00											
K	0.04	0.14	−0.03	0.06	0.15	1.00										
CO_3	−0.10	0.23	0.19	0.22	0.24	−0.32	1.00									
HCO_3	−0.14	−0.45	−0.45	−0.38	−0.46	−0.32	0.17	1.00								
SO_4	−0.01	0.65	0.53	0.63	0.63	0.33	0.05	−0.19	1.00							
Cl	0.00	0.99	0.94	0.95	0.99	0.10	0.25	−0.47	0.57	1.00						
Br	−0.03	0.99	0.93	0.94	0.99	0.13	0.30	−0.39	0.63	0.99	1.00					
SiO_2	−0.12	−0.12	−0.08	−0.02	−0.14	−0.10	−0.01	0.43	−0.12	−0.11	−0.12	1.00				
$\delta^{18}O$	0.00	0.77	0.66	0.66	0.79	0.32	−0.04	−0.63	0.60	0.75	0.73	−0.32	1.00			
δD	−0.01	0.74	0.61	0.60	0.77	0.28	−0.03	−0.56	0.58	0.72	0.70	−0.32	0.98	1.00		
SMI	−0.01	1.00	0.94	0.95	1.00	0.12	0.24	−0.48	0.60	1.00	0.99	−0.12	0.77	0.74	1.00	
GQI_{SWI}	−0.03	−0.97	−0.87	−0.90	−0.98	−0.29	−0.19	0.53	−0.64	−0.96	−0.96	0.18	−0.82	−0.79	−0.97	1.00

Three factors, with a total cumulative variance of about 80%, were assigned to explain changes made to groundwater (Table 4). Such factors are presented in two biplots to clearly illustrate their correlation with the different variables (Figure 12). The first factor f_1 (Figure 12a), with about 60% of the total variance, has high positive loading with the variables TDS, Ca, Mg, Na, Cl, and SO_4, $\delta^{18}O$, δD, and SMI and also has strong negative loading with GQI_{SWI}. This strong correlation can be interpreted as a result of different mechanisms. Among these are (1) rock–water interaction, (2) cation exchange, and (3) seawater intrusion. The second factor f_2 (Figure 12a) accounts for 11% of the total variance, which has a moderate positive loading with SO_4, $\delta^{18}O$, and δD as well as high positive loading with K. This suggests evaporation and dissolution of evaporites occurred in the shallower aquifers. The third factor f_3 (Figure 12b), with about 9% of the total variance, is

positively correlated with HCO_3 and SiO_2. This factor represents the freshening and the impact of the weathered silicate minerals on groundwater.

Table 4. Factor analysis from rotated component matrix.

Variable	Factor 1	Factor 2	Factor 3
pH	−0.059	−0.076	−0.524
TDS	**0.995**	−0.016	−0.056
Ca	**0.926**	−0.15	−0.096
Mg	**0.954**	−0.082	0.051
Na	**0.988**	−0.007	−0.084
K	0.143	**0.822**	0.002
CO_3	0.253	**−0.713**	0.061
HCO_3	−0.428	−0.339	**0.626**
SO_4	**0.676**	0.318	0.111
Cl	**0.985**	−0.064	−0.075
Br	**0.987**	−0.068	−0.025
SiO_2	−0.078	−0.07	**0.806**
$\delta^{18}O$	**0.787**	**0.371**	−0.313
δD	**0.756**	**0.353**	−0.299
SMI	**0.99**	−0.035	−0.079
GQI_{SWI}	**−0.968**	−0.11	0.13
Eigenvalue	9.74	1.93	1.15
Total variance %	60%	11%	9%
Cumulative %	60%	70%	80%

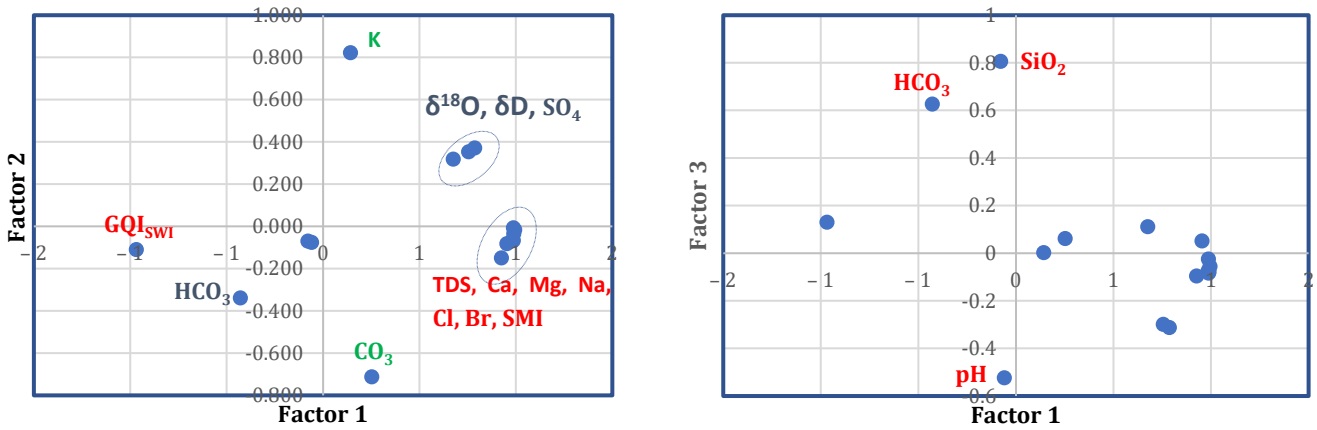

Figure 12. (**a**) Variable representation with F1 and F2 (high loading with F1 in red; high loading with F2 in green; medium loading with both in grey); (**b**) variable representation with F1 and F3 (high loading with F3 in red).

5.2.5. Groundwater Quality Index (GQI_{SWI}) and Seawater Mixing Index (SMI)

The GQI_{SWI} varies from 0 to 100, and the values above 75 can be considered as freshwater, while when below 50, groundwater is classified as saline or seawater. If groundwater has GQI_{SWI} values ranging between 50 and 75, it will be deemed as mixed water. The calculated GQI_{SWI} values presented in Table 5 reveal that the study area is dominated by saline and mixed groundwater (55 and 41%, respectively), followed by saltwater (4%).

Table 5. Classification of groundwater based on GQI_{SWI} and SMI.

Classification According to GQI_{SWI}	GQI_{SWI}		Classification According to SMI	SMI	
	Range	Sample%		Range	Sample%
Freshwater	75–100	0%	Freshwater	less than 1	90%
Mixed groundwater	50–75	41%	Moderately polluted	1–6	10%
Saline groundwater	10–50	55%	Seriously polluted	6–10	0%
Saltwater	0–10	4%	Seawater	10–150	0%

The SMI was calculated when the cumulative probability percentages of Cl, SO_4, Na, and Mg ions were plotted against their concentration in mg/L (Figure 13). The inflection points of each plot characterize the threshold values (T) of each ion that were substituted in Equation (5) to calculate the SMI values for each groundwater sample. If the SMI value was more than 1, the water may have been influenced by seawater mixing [69,70]. The results of the calculated SMI show that about 90% (52 samples) of the groundwater samples are of meteoric origin, and the remaining 10% (6 samples) are related to saline groundwater. This hypothesis is compatible with the results obtained from the ion ratios and stable isotopes analyses. It should be noted that the variation in SMI and GQI_{SWI} calculated values is due to how each method characterizes groundwater. In other words, the SMI considers seawater as a pollutant, and its percentage in groundwater is calculated, so that if the index value exceeds unity, this indicates seawater intrusion. The GQI index, on the other hand, classifies groundwater based on its origin and takes into account the changes that occurred as a result of various geochemical processes, including intrusion of sea water.

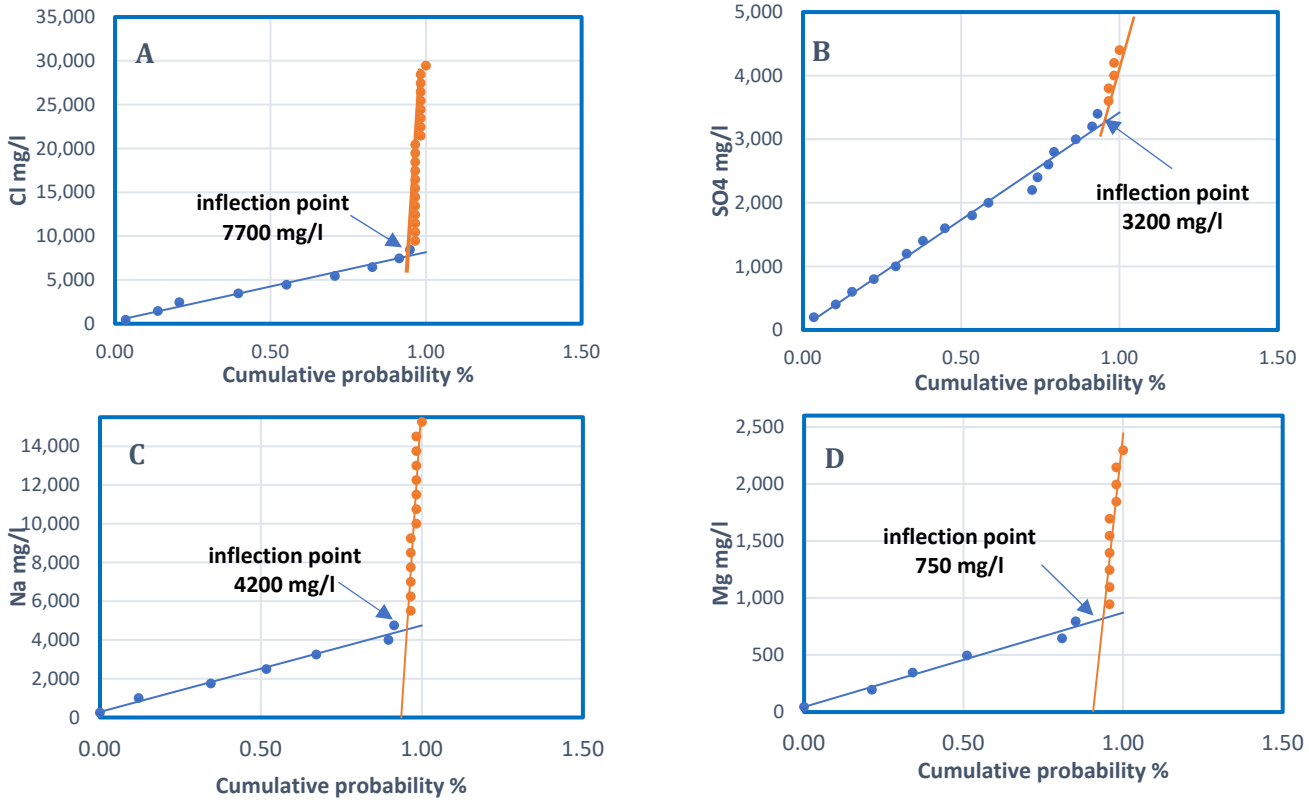

Figure 13. Threshold values (T) of (**A**) Cl, (**B**) SO_4, (**C**) Na, and (**D**) Mg in the studied groundwater samples. The intersection of the background concentration (highlighted in blue) and the trend line representing the anomalous concentrations (highlighted in orange) indicates the regional threshold of relevant element.

The spatial distribution of the groundwater quality index (GQI_{SWI}) as well as the seawater mixing index (SMI) were used as complementary tools to delineate the salinization zones in accordance with the extent to which groundwater was affected either by freshwater mixing with seawater or rock–water interaction. According to the spatial distribution maps for GQI_{SWI} and SMI (Figure 14A,B), it was revealed that almost all the groundwater in the study area is mainly of meteoric origin, which in turn reaches a progressive evolutionary stage due to the interaction with marine sediments and mixing with salt water. Patches that have undergone saltwater intrusion were identified in some locations along the shoreline of the Mediterranean Sea. However, saline water was also identified in some other inland locations west of the study area, about 12.5 km away from the sea.

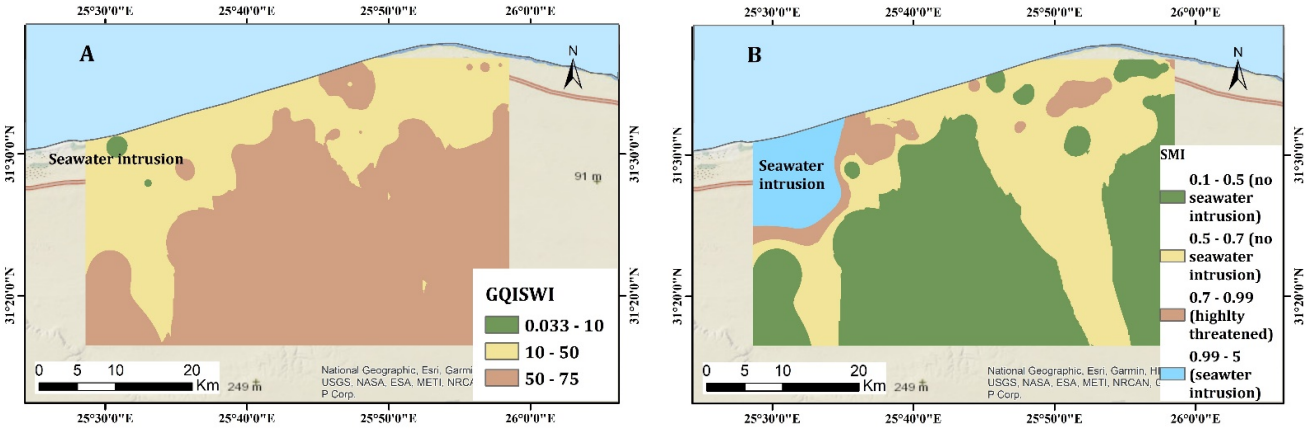

Figure 14. Iso-contour map of GQI_{SWI} and SMI. Figures (**A**,**B**) indicated the areas, which are thought to be affected by seawater intrusion based on GQI_{SWI}, and SMI calculations, respectively.

6. Conclusions

This paper highlighted the different processes and mechanisms impacting groundwater salinization using multi-hydrochemical parameters and stable isotopes. The groundwater in the study area is classified as brackish, saline, and highly saline water. Different methods, including ion ratio relationships, isotope bivariate plots, evolution diagrams, and statistical analyses, were applied to recognize the main geochemical processes controlling the salinization processes. According to Gibbs classifications, groundwaters are dominated by evaporation followed by rock–water interaction. The HFE-D indicated mixing with saline water and the occurrence of both reverse and direct cation exchange. The correlation of the ion ratios Na/Cl, Mg/Ca, SO_4/Cl, and Br/Cl with TDS indicates the effect of marine sediments and seawater as well as the anthropogenic activities on some of the studied groundwater samples. Furthermore, the $Na_{deficit}$ and Ca_{excess} bi-plot revealed different processes, including halite dissolution, cation exchange, and seawater evaporation after calcite precipitation. The $\delta^{18}O$ vs. δD and TDS vs. $\delta^{18}O$ relationships revealed that some samples were exposed to mixing with seawater and/or fractionation during the evaporation from shallow groundwater aquifers. The factors extracted by PCA suggest the aforementioned processes, in addition to the impact of freshening and silicate weathering on groundwater. The mixing with seawater was confirmed in some locations along the coastline and extended to about 12.5 km away from shore in the Bqabaq area. Additionally, statistical analyses as well as hydrogen and oxygen-18 stable isotope relationships identified the effect of recharge by rainwater in few locations. The findings from this study can be used to enhance our understanding of the different hydrogeochemical processes that led to the deterioration in the groundwater quality. Moreover, it sheds light on the locations that have experienced groundwater quality deterioration as well as other areas that are not or are little affected by seawater intrusion. This will enable the decision makers to take the necessary measures to use groundwater in those areas in a way that ensures its sustainability and does not lead to any further deterioration.

Funding: This research received no external funding.

Data Availability Statement: Data available upon request from the corresponding author.

Acknowledgments: The author would like to express his deepest gratitude to Viorel Atudorei, Center for Stable Isotopes, University of New Mexico, USA, for conducting the stable isotopic analyses. Many thanks also to the anonymous reviewers, whose valuable comments enriched this manuscript, and to the editors of the Sustainability Journal. Special thanks and appreciation to Mansoura University for funding this research paper. Sincere thanks to Jean Bahr for editing the manuscript's language as a native English speaker.

Conflicts of Interest: The author declares no conflict of interest.

References

1. Gaaloul, N.; Pliakas, F.; Kallioras, A.; Schuth, C.; Marinos, P. Simulation of Seawater Intrusion in Coastal Aquifers: Forty Five'Years exploitation in an Eastern Coast Aquifer in NE Tunisia. *Open Hydrolgeol. J.* **2012**, *6*, 31–44. [CrossRef]
2. McInnis, D.; Silliman, S.E. Geoelectrical investigation of the freshwater–saltwater interface in coastal Benin, West Africa. In Proceedings of the American Geophysical Union, Fall Meeting, San Francisco, CA, USA, 13–17 December 2010.
3. Edmunds, W.M.; Milne, C.J. *Palaeowaters in Coastal Europe: Evolution of Groundwater since the Late Pleistocene*; Geological Society of London: London, UK, 2001.
4. De Montety, V.; Radakovitch, O.; Vallet-Coulomb, C.; Blavoux, B.; Hermitte, D.; Valles, V. Origin of groundwater salinity and hydrogeochemical processes in a confined coastal aquifer: Case of the Rhone delta (Southern France). *Appl. Geochem.* **2008**, *23*, 2337–2349. [CrossRef]
5. Somay, M.A.; Gemici, U. Assessment of the salinization process at the coastalarea with hydrogeochemical tools and geographical information systems (GIS): Selcuk Plain, Izmir, Turkey. *Water Air Soil Pollut.* **2009**, *201*, 55–74. [CrossRef]
6. Kim, Y.; Lee, K.S.; Koh, D.C.; Lee, D.H.; Lee, S.G.; Park, W.B.; Koh, G.W.; Woo, N.C. Hydrogeochemical and isotopic evidence of groundwater salinization in a coastal aquifer: A case study in Jeju volcanic island, Korea. *J. Hydrol.* **2003**, *270*, 282–294. [CrossRef]
7. Tijani, M.N. Evolution of saline waters and brines in the Benue-Trough. Nigeria. *Appl. Geochem.* **2004**, *19*, 1355–1365. [CrossRef]
8. Ghabayen, S.M.S.; McKee, M.; Kemblowski, M. Ionic and isotopic ratios for identification of salinity sources and missing data in the Gaza aquifer. *J. Hydrol.* **2006**, *318*, 360–373. [CrossRef]
9. Mirzavand, M.; Ghasemieh, H.; Sadatinejad, S.J.; Bagheri, R.; Clark, I.D. Saltwater intrusion vulnerability assessment using AHPGALDIT Model in Kashan plain aquifer as critical aquifer in a semi-arid region. *Desert* **2018**, *32*, 255–264.
10. Pérez-Martín, M.A.; Estrela, T.; Andreu, J.; Ferrer, J. Modeling water resources and river-aquifer interaction in the Júcar River Basin, Spain. *Water Resour. Manag.* **2014**, *28*, 4337–4358. [CrossRef]
11. Masciopinto, C. Simulation of coastal groundwater remediation: The case of Nardò fractured aquifer in Southern Italy. *Environ. Model. Softw.* **2006**, *21*, 85–97. [CrossRef]
12. Mjemah, I.C.; Van Camp, M.; Walraevens, K. Groundwater exploitation and hydraulic parameter estimation for a Quaternary aquifer in Dar-es-Salaam, Tanzania. *J. Afr. Earth Sci.* **2009**, *55*, 134–146. [CrossRef]
13. Van Camp, M.; Mtoni, Y.E.; Mjemah, I.C.; Bakundukize, C.; Walraevens, K. Investigating seawater intrusion due to groundwater pumping with schematic model simulations: The example of the Dar Es Salaam coastal aquifer in Tanzania. *J. Afr. Earth Sci.* **2014**, *96*, 71–78. [CrossRef]
14. Bear, J.; Cheng, A.; Sorek, S.; Ouazar, D.; Herrera, I. *Seawater Intrusion in Coastal Aquifers Concepts, Methods and Practices*; Springer: Berlin/Heidelberg, Germany, 1999.
15. Barlow, P.M.; Reichard, E.G. Saltwater intrusion in coastal regions of North America. *Hydrogeol. J.* **2010**, *18*, 247–260. [CrossRef]
16. Werner, A.D. A review of seawater intrusion and its management in Australia. *Hydrogeol. J.* **2010**, *18*, 281–285. [CrossRef]
17. Custodio, E. Coastal aquifers of Europe: An overview. *Hydrogeol. J.* **2010**, *18*, 269–280. [CrossRef]
18. Bocanegra, E.; Da Silva, G.C.; Custodio, E.; Manzano, M.; Montenegro, S. State of knowledge of coastal aquifer management in South America. *Hydrogeol. J.* **2010**, *18*, 261. [CrossRef]
19. Steyl, G.; Dennis, I. Review of coastal-area aquifers in Africa. *Hydrogeol. J.* **2010**, *18*, 217–225. [CrossRef]
20. UN—United Nations. *Water for People, Water for Life*; UN World Development Report (WWDR); UN: New York, NY, USA, 2003.
21. WHO—World Health Organization. *Guidelines for Drinking-Water Quality: First Addendum to Third Edition*; WHO: Geneva, Switzerland, 2006; Volume 1 Recommendations.
22. El Shamy, I. The Geology of Soil and Water Resources in El Daba'a Area. Master's Thesis, Faculty of Science, Cairo University, Giza, Egypt, 1968.
23. Selim, A.A. Geology of El-Salum Area. Ph.D. Thesis, Faculty of Science, Alexandria University, Alexandria, Egypt, 1969.
24. Rizk, Z.E. Geological and Hydrogeological Studies on the North Wetern Coast of Egypt. Master's Thesis, Faculty of Science, Menofia University, Shibin el Kom, Egypt, 1982. Unpublished.
25. Hammad, F.A. The Geology of Soils and Water Resources in the Area between Ras El Hekma and Ras El Rum (Western Mediterranean Littoral Zone, Egypt). Ph.D. Thesis, Faculty of Science, Cairo University, Giza, Egypt, 1972.

26. Misak, R. Geomorphology and Geology of the Area between El Daba'a and Ras El Hekma, Western Mediterranean Coastal Zone, Egypt. Master's Thesis, Ain Shamas University, Cairo, Egypt, 1974.
27. Mousa, B.M. Geomorphology and Subsurface Geology of the Area between El Alamein and Qattara Depression, Northern Western Desert, Egypt. Master's Thesis, Faculty of Science, Ain Shams University, Cairo, Egypt, 1976.
28. AbdelMogheeth, S. Sedimentology, Geochemistry and Evaluations of the Marmarica Limestone, Western Desert, Egypt. Ph.D. Thesis, Faculty of Science, Al Azhar University, Cairo, Egypt, 1968.
29. Atwa, S.M. Hydrology and Hydrogeochemistry of the Northwestern Coast of Egypt. Ph.D. Thesis, Faculty of Science, Alexandria University, Alexandria, Egypt, 1979.
30. Salem, A.A.; Mohamed, A.H. Hydrogeological studies of the groundwater aquifers in El Sallum depression, Northwestern coast, Egypt. *Sedimentol. Egypt.* **2011**, *19*, 97–112.
31. Aureli, A.; Ganoulis, J.; Margat, J. *Groundwater Resources in the Mediterranean Region: Importance, Uses and Sharing*; UNESCO International Hydrological Programme (IHP): Paris, France, 2008; pp. 96–105.
32. Hammad, F.A. The Geology of Water Supplies in Ras El Hekma Area, Western Mediterranean Coastal Zone, Egypt. Master's Thesis, Cairo University, Giza, Egypt, 1966.
33. Guo, X.; Feng, Q.; Liu, W.; Li, Z.; Wen, X.; Si, J.; Jia, B. Stable isotopic and geochemical identification of groundwater evolution and recharge sources in the arid Shule River Basin of Northwestern China. *Hydrol. Process.* **2015**, *29*, 4703–4718. [CrossRef]
34. Budiyanto, E.; Muzayanah; Prasetyo, K. Karst Groundwater Vulnerability and Risk to Pollution Hazard in the Eastern Part of Gunungsewu Karst Area. *IOP Conf. Ser. Earth Environ. Sci.* **2020**, *412*, 012020. [CrossRef]
35. Richter, B.C.; Kreitler, C.W. *Geochemical Techniques for Identifying Sources of Ground-Water Salinization*; CRC Press: Boca Raton, FL, USA, 1993.
36. Smith, A.J.; Turner, J.V. Density-dependent surface water-groundwater interaction and nutrient discharge in the Swan-Canning Estuary. *Hydrol. Process.* **2001**, *15*, 2595–2616. [CrossRef]
37. Simpson, M.J.; Clement, T.P. Improving the worthiness of the Henry problem as a benchmark for density-dependent groundwater flow models. *Water Resour. Res.* **2004**, *40*, W01504. [CrossRef]
38. Narayan, K.A.; Schleeberger, C.; Bristow, K.L. Modelling seawater intrusion in the Burdekin Delta Irrigation Area, North Queensland, Australia. *Agr. Water Manag.* **2007**, *89*, 217–228. [CrossRef]
39. Werner, A.D.; Simmons, C.T. Impact of sea-level rise on seawater intrusion in coastal aquifers. *Groundwater* **2009**, *47*, 197–204. [CrossRef] [PubMed]
40. Edmunds, W.M.; Walton, N.R.G. A geochemical and isotopic approach torecharge evaluation in semi-arid zones, past and present. In *Arid-Zone Hydrology, Investigations with Isotope Techniques*; International Atomic Energy Agency: Vienna, Austrian, 1980; pp. 47–68.
41. Simmers, I. Natural Groundwater Recharge Estimation in (Semi-)Arid Zones; Some State of-the-art Observations. In *Sahel Forum on the State-of the-Art of Hydrology and Hydrogeology in the Arid and Semi-Arid Areas of Aji-Ica*; Stout, G.E., Demissie, M., Eds.; UNESCO: New York, NY, USA, 1990; pp. 373–386.
42. Edmunds, W.M.; Gaye, C.B. Estimating the spatial variability of groundwater recharge in the Sahel using chloride. *J. Hydrol.* **1994**, *156*, 47–59. [CrossRef]
43. Clark, I.D.; Fritz, P. *Environmental Isotopes in Hydrogeology*; Lewis Publishers: Boca Raton, FL, USA, 1997.
44. Mook, G.W. *Environmental Isotopes in the Hydrological Cycle*; IHP-V Technical Document in Hydrology No. 39 VI; UNESCO: Paris, France, 2001.
45. Vengosh, A. *Salinization and Saline Environments, Treatise on Geochemistry*, 2nd ed.; Elsevier Ltd.: Amsterdam, The Netherlands, 2013; 333p. [CrossRef]
46. Raslan, S.M. Geomorpholiogical and Hydrogeological Studies on Some Localities Along the Northwestern Coast of Egypt. Master's Thesis, Faculty of Science, Menoufia University, Shibin el Kom, Egypt, 1995; p. 172.
47. Khalil, M.M. Origin, Genesis, Formation and classification of Sidi Barrani Soils, Northwestern Coastal Zone. Master's Thesis, Faculty of Agriculture, Zagazig University, Cairo, Egypt, 2008.
48. El Shazly, M.M. Geology, Pedology and Hydrogeology of Mersa Matruh Area, Western Mediterranean Littoral, U.A.R. Ph.D. Thesis, Faculty of Science, Cairo University, Cairo, Egypt, 1964.
49. Ali, A.O.; Rashid, M.; El Naggar, S.; Abdul Al, A. Water harvesting options in the drylands at different spatial scales. *Land Use Water Resour. Res.* **2007**, *7*, 1–13.
50. El Sabri, M.A.; Salem, W.M. Management of groundwater resources in El Saloum depression, Western Desert, Egypt. *Ann. Geol. Surv. Egypt* **2016**, *XXXIII*, 193–210. Available online: https://www.researchgate.net/profile/Mohamed-El-Sabri/publication/333208963_Annalas_Geol_Surv_Egypt_V_XXXIII_2016_pp_197-213 (accessed on 3 November 2022).
51. Morad, N.; Masoud, M.; Abdel Moghith, S. Hydrologic factors controlling groundwater salinity in northwestern coastal zone. *Egypt. J. Earth Syst. Sci.* **2014**, *123*, 1567–1578. [CrossRef]
52. Yousif, M.; Oguchi, T.; Anazawa, K.; Ohba, T. Framework for Investigation of Karst Aquifer in an Arid Zone, Using Isotopes, Remote Sensing and GIS Applications: The Northwestern Coast of Egypt. *Environ. Process.* **2015**, *2*, 37–60. [CrossRef]
53. Rainwater, F.H.; Thatcher, L.L. *Methods for Collection and Analysis of Water Samples*; Paper No. 1454; U.S. Geological Survey: Washington, DC, USA, 1960; p. 301.

54. Fishman, M.J.; Friedman, L.C. *Methods for Determination of Inorganic Substances in Water and Fluvial Sediments*; Open-File Report, 85–495; U.S. Geological Survey: Denver, CO, USA, 1985; Volume 5, Chapter A1.
55. ASTM (American Society for Testing and Materials). *Annual Book of ASTM Standards*; ASTM: Baltimore, MD, USA, 2002; Volume 11, 939p.
56. Coplen, T.B.; Wildman, J.D.; Chen, J. Improvements in the gaseous hydrogen-water equilibrium technique for hydrogen isotope ratio analysis. *Anal. Chem.* **1991**, *63*, 910–912. [CrossRef]
57. Coplen, T.B. Reporting of stable hydrogen carbon and oxygen isotopic abundances. *Pure Appl. Chem.* **1994**, *66*, 273–276. [CrossRef]
58. Gibbs, R.J. Mechanisms controlling world water chemistry. *Science* **1970**, *170*, 1088–1090. [CrossRef] [PubMed]
59. Gimenez Forcada, E. Dynamic of seawater interface using hydro chemical facies evolution diagram. *Groundwater* **2010**, *48*, 212–216. [CrossRef]
60. Najib, S.; Fadili, A.; Mehdi, K.; Riss, J.; Makan, A. Contribution of hydrochemical and geoelectrical approaches to investigate salinization process and seawater intrusion in the coastal aquifers of Chaouia, Morocco. J. *Contam. Hydrol.* **2017**, *198*, 24–36. [CrossRef] [PubMed]
61. Naseem, S.; Bashir, E.; Ahmed, P.; Rafique, T.; Hamza, S.; Kaleem, M. Impact of Seawater Intrusion on the Geochemistry of Groundwater of Gwadar District, Balochistan and Its Appraisal for Drinking Water Quality. *Arab. J. Sci. Eng.* **2018**, *43*, 281–293. [CrossRef]
62. Gimenez-Forcada, E.; Roman, F.J.S.S. An Excel Macro to Plot the HFE-Diagram to Identify Seawater Intrusion Phases. *Groundwater* **2014**, *53*, 819–824. [CrossRef] [PubMed]
63. Davis, J.C. *Statistics and Data Analysis in Geology*; John Wiley & Sons, Inc.: New York, NY, USA, 2002.
64. Rao, N.S.; Devadas, D.J.; Rao, K.V.S. Interpretation of groundwater quality using principal component analysis from Anantapur district, Andhra Pradesh, India. *Environ. Geosci.* **2006**, *13*, 239–259.
65. Kaiser, H.F. The varimax criteria for analytical rotation in factor analysis. *Psychometrika* **1958**, *23*, 187–200. [CrossRef]
66. Tomaszkiewicz, M.; Najm, M.A.; El-Fadel, M. Development of a groundwater quality index for seawater intrusion in coastal aquifers. *Environ. Model. Softw.* **2014**, *57*, 13–26. [CrossRef]
67. Piper, A.M. A graphic procedure in the geochemical interpretation of water-analyses. *Eos Trans. Am. Geophys. Union.* **1944**, *25*, 914–928. [CrossRef]
68. Appelo, C.A.J.; Postma, D. *Geochemistry, Groundwater and Pollution*, 2nd ed.; CRC Press: London, UK, 2005; 683p.
69. Park, S.-C.; Yun, S.-T.; Chae, G.-T.; Yoo, I.-S.; Shin, K.-S.; Heo, C.-H.; Lee, S.-K. Regional hydrochemical study on salinization of coastal aquifers, western coastal area of South Korea. *J. Hydrol.* **2005**, *313*, 182–194. [CrossRef]
70. Sinclair, A. Selection of threshold values in geochemical data using probability graphs. *J. Geochem. Explor.* **1974**, *3*, 129–149. [CrossRef]
71. USGS (United States Geological Survey). Water Science School, Saline Water and Salinity. 2018. Available online: https://www.usgs.gov/special-topics/water-science-school/science/saline-water-and-salinity (accessed on 3 November 2022).
72. Sukhija, B.S.; Varma, V.N.; Nagabhushanam, P.; Reddy, D.V. Differentiation of paleomarine and modern seawater intruded salinities in coastal groundwaters (of Karaikal and Tanjavur, India) based on inorganic chemistry, organic biomarker fingerprintsand radiocarbon dating. *J. Hydrol.* **1996**, *174*, 173–201. [CrossRef]
73. El Moujabber, M.; BouSamra, B.; Darwish, T.; Atallah, T. Comparison of different indicators for groundwater contamination by seawater intrusion on the Lebanese coast. *Water Resour. Manag.* **2006**, *20*, 161–180. [CrossRef]
74. Jacobson, R.L.; Langmuir, D. The chemical history of some spring waters in carbonate rocks. *Groundwater* **1970**, *8*, 5–9. [CrossRef]
75. Jones, B.F.; Vengosh, A.; Rosenthal, E.; Yechieli, Y. Chapter 3: Geochemical Investigations. In *Seawater Intrusion in Coastal Aquifers–Concepts, Methods and Practices*; Bear, J., Cheng, A.H.D., Sorek, S., Ouazar, D., Herrera, I., Eds.; Kluwer Academic Publishers: Dordrecht, The Netherlands, 1999; pp. 51–72.
76. Andreasen, D.C.; Fleck, W.B. Use of bromide: Chloride ratios to differentiate potential sources of chloride in a shallow, unconfined aquifer affected by brackish-water intrusion. *Hydrogeol. J.* **1997**, *5*, 17–26. [CrossRef]
77. Hem, J.D. *Study and Interpretation of the Chemical Characteristics of Natural Wate*; USGS Water-Supply Paper; USGS: Reston, VA, USA, 1992; Volume 2254, 263p.
78. Davisson, M.L.; Presser, T.S.; Criss, R.E. Geochemistry of tectonically expelled fluids from the northern coast ranges, rumsey hills, california, USA. *Geochim. Cosmochim. Acta* **1994**, *58*, 1687–1699. [CrossRef]
79. Davisson, M.L.; Criss, R.E. Na-Ca-Cl relations in basinal fluids. *Geochim. Cosmochim. Acta* **1996**, *60*, 2743–2752. [CrossRef]
80. Parkhurst, D.L.; Appelo, C. Description of input and examples for PHREEQC version 3—A computer program for speciation, batch-reaction, one-dimensional transport, and inverse geochemical calculations. *US Geol. Surv. Tech. Methods* **2013**, *6*, A43–497.
81. Geyh, M. Environmental Isotopes in the Hydrological Cycle Principles and Applications, Principales and Applications, IAEA/UNESCO; Volume 4, 424p. 2000. Available online: https://www.naweb.iaea.org/napc/ih/documents/global_cycle/Environmental%20Isotopes%20n%20the%20Hyrological%20Cycle%20Vol%204.pdf (accessed on 9 September 2022).
82. Craig, H. Isotopic variations in meteoric waters. *Science* **1961**, *133*, 1702–1703. [CrossRef]
83. Gat, J.R.; Carmi, I. Evolution of the isotopic composition of atmospheric waters in the Mediterranean Sea area. *J. Geophys. Res.* **1970**, *75*, 3039–3048. [CrossRef]
84. Olive, P. *Introduction to Isotope Hydrology, Geodynamic Research Center*; Didactic and Pedagogical Publishing House: Bucharest, Romania, 1996; 126p. (in French)